7-21-2021

The antimalarial MMV688533 provides potential for single-dose cures with a high barrier to

James M. Murithi
Columbia University Irving Medical Center

Cécile Pascal
Sanofi, Infectious Diseases Therapeutic Area

Jade Bath
Columbia University Irving Medical Center

Xavier Boulenc
Sanofi Pasteur

Nina F. Gnädig
Columbia University Irving Medical Center

See next page for additional authors

https://doi.org/10.1126/scitranslmed.abg6013

The antimalarial MMV688533 provides single-dose cures with a high barrier to *Plasmodium falciparum* parasite resistance

James M. Murithi[1§], Cécile Pascal[2δ¶], Jade Bath[1], Xavier Boulenc[3¶], Nina F. Gnädig[1], Charisse F.A. Pasaje[4], Kelly Rubiano[1], Tomas Yeo[1], Sachel Mok[1], Sylvie Klieber[2], Paul Desert[3], Maria Belen Jimenez-Diaz[5], Jutta Marfurt[6], Mélanie Rouillier[7], Mohammed Cherkaoui[7], Nathalie Gobeau[7], Sergio Wittlin[8,9], Anne-Catrin Uhlemann[10], Ric N. Price[6,11,12], Grennady Wirjanata[13], Rintis Noviyanti[14], Patrick Tumwebaze[15], Roland A. Cooper[16], Philip J. Rosenthal[17], Laura M. Sanz[18], Francisco Javier Gamo[18], Jayan Joseph[19], Shivendra Singh[19], Sridevi Bashyam[19], Jean Michel Augereau[2], Elie Giraud[2¶], Tanguy Bozec[2¶], Thierry Vermat[2¶], Gilles Tuffal[2], Jean-Michel Guillon[2], Jérôme Menegotto[2¶], Laurent Sallé[2], Guillaume Louit[2], Marie-José Cabanis[2], Marie Françoise Nicolas[2], Michel Doubovetzky[2], Rita Merino[2†], Nadir Bessila[2¶], Iñigo Angulo-Barturen[5], Delphine Baud[7], Lidiya Bebrevska[7], Fanny Escudié[7ʃ], Jacquin C. Niles[4], Benjamin Blasco[7$], Simon Campbell[7], Gilles Courtemanche[20], Laurent Fraisse[2ʃ], Alain Pellet[2¶], David A. Fidock[1,10]*, Didier Leroy[7]*

[1]Department of Microbiology and Immunology, Columbia University Irving Medical Center, New York, NY, USA. [2]Sanofi, Infectious Diseases Therapeutic Area, Marcy l'Etoile, France. [3]Sanofi Pasteur, Lyon, France. [4]Department of Biological Engineering, Massachusetts Institute of Technology, Cambridge, MA, USA.[5]The Art of Discovery, Bizkaia, Basque Country, Spain. [6]Global and Tropical Health Division, Menzies School of Health Research and Charles Darwin University, Darwin, Australia. [7]Medicines for Malaria Venture, Geneva, Switzerland. [8]Department of Medical Parasitology and Infection Biology, Swiss Tropical and Public Health Institute, CH-4002 Basel, Switzerland. [9]Universität Basel, CH-4003 Basel, Switzerland. [10]Division of Infectious Diseases, Department of Medicine, Columbia University Irving Medical Center, New York, NY 10032, USA. [11]Centre for Tropical Medicine and Global Health, Nuffield Department of Medicine, University of Oxford, Oxford, United Kingdom. [12]Mahidol-Oxford Tropical Medicine Research Unit, Faculty of

Tropical Medicine, Mahidol University, Bangkok, Thailand. [13] Global Health and Tropical Medicine Division, Menzies School of Health Research, Charles Darwin University, Darwin, Northern Territory, Australia. [14]Eijkman Institute for Molecular Biology, Jakarta, Indonesia. [15]Infectious Diseases Research Collaboration, Kampala, Uganda. [16]Department of Natural Sciences and Mathematics, Dominican University of California, San Rafael, CA, USA. [17]Department of Medicine, University of California, San Francisco, CA, USA. [18]Global Health Pharma Research Unit, GSK, Tres Cantos, Madrid, Spain. [19]Syngene International Ltd. Bangalore, India. [20]Bioaster, Paris, France.

Current addresses: [¶]Evotec Infectious Diseases Lyon, France. [ʃ]Drugs for Neglected Diseases initiative, Geneva, Switzerland. [$]Global Antibiotic Research and Development Partnership, Geneva, Switzerland.

[†]In memoriam.

[§]Co-first authors.

*Co-corresponding authors, DAF: df2260@cumc.columbia.edu; DL: leroyd@mmv.org

One Sentence Summary: We report an acylguanidine preclinical candidate with efficacy, resistance and pharmacological features compatible with single low-dose malaria cure.

ABSTRACT

The emergence and spread of *Plasmodium falciparum* resistance to first line antimalarials creates an imperative to identify and develop novel potent chemotypes. Here we report the identification of MMV688533, an acylguanidine discovered using an orthology-based screen, which displays fast parasite clearance in vitro and is not cross-resistant with known antimalarials. In a *P. falciparum* SCID mouse model, MMV688533 displays a long-lasting pharmacokinetic profile and excellent safety. Selection studies revealed a very low propensity for resistance, with modest loss of potency mediated via point mutations in PfACG1 and PfEHD. These proteins are implicated in intracellular trafficking, lipid utilization and endocytosis, suggesting interference with these pathways as a novel mode of action. This declared preclinical candidate offers the potential for a single low-dose cure for malaria.

INTRODUCTION

Worldwide, malaria mortality and incidence were estimated to decrease by 60% and 37% respectively from 2000 to 2015. This positive trend came to an end in 2016, with cases and deaths plateauing and 229 million cases and 409,000 deaths estimated in 2019 (*1*). *P. falciparum* parasite resistance to first-line Artemisinin-based Combination Therapies (ACTs) continues to be on the rise in Southeast Asia and now threatens Africa (*2-4*). Despite extensive worldwide initiatives, malaria drug discovery and development efforts have encountered major obstacles to identifying new agents with novel modes of antiplasmodial action that do not readily succumb to parasite resistance (*5*).

To address these barriers, we applied a novel drug discovery approach leveraging research and development programs on human diseases at Sanofi. While classic approaches rely on the identification of compounds that are both potent and specific against *Plasmodium* parasites, our strategy first identified *Plasmodium*-active compounds from a library of chemical matter with known activity against human targets selected from discovery programs through to Phase III clinical trials. Compounds active against *P. falciparum* asexual blood-stage parasites were then chemically optimized to increase antiplasmodial specificity and reduce host toxicity risks. Our approach led to the identification of several highly potent new chemical series, including the acylguanidines ultimately exemplified by MMV688533. This molecule was shown to act via a novel mode of action that allowed *P. falciparum* parasites to acquire only low-grade resistance under drug pressure.

RESULTS

Identification of acylguanidines as a potent antiplasmodial chemical series with promising physicochemical properties

A bioinformatics-mediated analysis of Sanofi drug discovery programs led to the selection of 450 compounds active against one of 33 human targets for which putative orthologs were found in *P. falciparum, Trypanosoma brucei*, *Trypanosoma cruzi*, and/or *Leishamania donovani*. We also included 350 compounds active against any one of 28 Sanofi high-priority human targets. Screening of these 800 compounds against cultured *P. falciparum* asexual blood stage parasites identified 120 compounds whose half-maximal growth inhibition concentration (IC_{50}) was ≤ 1 μM, corresponding to a 15% hit rate. As a comparison, classical random screening approaches have earlier yielded 0.35-0.68% hit rates (*6-8*), highlighting the benefit of our drug discovery strategy. We then applied hit selection criteria including suitable physicochemical properties (https://www.mmv.org/research-development/information-scientists) and IC_{50} values <1 μM against a panel of drug-sensitive or -resistant *P. falciparum* strains, and screened an additional set of 800 analogs of preferred hits to expand Structure-Activity Relationships (SAR) (*9*). This work yielded six chemical scaffolds for medicinal chemistry optimization. Here we describe the acylguanidine series, which includes the initial hit MMV668603 that was exquisitely potent against *P. falciparum* NF54 asexual blood stages, with an IC_{50} of 1.7 nM. This hit originated from the dimerization of a compound chemically related to Cariporide, an inhibitor of human Na^+/H^+ exchanger isoform 1 (NHE1) that has anticancer and cardioprotective properties (*10, 11*). A hit to lead optimization program, including SAR studies, led to the intermediate compound MMV669851 and the eventual preclinical candidate MMV688533 (**Fig. 1A**). Compared to MMV668603, the candidate MMV688533 does not contain a diazo moiety,

shows improved solubility (from <10 µg/mL to >1,000 µg/mL at pH 1) and intestinal permeability, and retains potent antiplasmodial activity (**Fig. 1A; Tables S1A, S1B**).

MMV688533 displayed fast asexual blood stage parasite killing rate and high potency against *P. falciparum* and *P. vivax* strains in vitro and ex vivo

MMV688533 was highly potent against multiple *P. falciparum* strains, with IC_{50} values in the low nanomolar range and no evidence of reduced potency against parasite lines resistant to antimalarials currently in the clinic or in development (**Table S1C**). These data suggest that MMV688533 might have a distinct mode of antiplasmodial action. MMV688533 also showed excellent ex vivo activity against asexual blood stage parasites from fresh *P. falciparum* isolates from Ugandan patients (median IC_{50} = 1.3 nM, range 0.02 – 6.3 nM, N=143). In Papua Indonesia, where both *P. falciparum* and *P. vivax* are endemic, MMV688533 remained potent in ex vivo assays, with similar IC_{50} values against both parasite species (medians of 18.9 and 12.0 nM respectively; **Table 1**). MMV688533 was as potent if not more so than either chloroquine or piperaquine against *P. falciparum* and *P. vivax* clinical field isolates (**Table 1**). This compound did not show potent activity against *P. falciparum* liver stages or male and female gametes (**Table S1D**).

MMV688533 displayed a fast-killing profile in the parasite reduction rate (PRR) assay (*12*), as demonstrated by a $\log_{10}$ PRR of nearly 5, corresponding to a decrease of parasitemia by nearly 5 orders of magnitude during a single 48 h intra-erythrocytic developmental cycle (**Fig. 1B**). This profile is similar to dihydroartemisinin, the active metabolite of artemisinins that constitute the fastest-acting class of antimalarials available to date (*13*). This compound displayed very rapid

parasite killing when tested over the range of 1–30× IC_{50} (**Fig. 1C**), as well as very low cytotoxicity (**Table S1E**).

MMV688533 displayed fast and potent in vivo efficacy and favorable in vitro ADME and in vivo PK properties

MMV688533 was highly efficacious in the NOD-SCID IL2Rγ^{null} mouse model of *P. falciparum* asexual blood-stage infection (*14*), with a single oral dose of 5 mg/kg resulting in a rapid reduction in parasitemia to below the limit of detection within 48 h, followed by recrudescence to 1% by day 18. By comparison, vehicle-treated mice attained a lethal parasitemia of 8-10% by day 5 (**Fig. 1D**). These data predicted an ED_{90} of 2 mg/kg, corresponding to the single dose required to reduce parasitemia by >90% by day 7 compared to vehicle-treated mice (**Fig. 1D, 1E; Table S1F**). Four consecutive daily doses of 0.9 mg/kg produced >90% reduction in parasitemia by day 7 (data not shown). Importantly, one dose of at least 5 mg/kg MMV688533 cleared parasites as rapidly as 50 mg/kg dihydroartemisinin **(Fig. 1D**). Pharmacokinetic-pharmacodynamic (PK/PD) modeling predicted an in vivo minimal parasiticidal concentration of 20.3 ng/mL (**Table S1G**).

PK studies indicated a low plasma clearance (C_L) in mice, rats and dogs (**Table S1H**). When tested on purified cytochrome P450 enzymes, MMV688533 did not show high inhibitory potency (**Table S1I**). MMV688533 also displayed a moderate to high volume of distribution (V_{ss}: 1.4 L/kg in mice, 4.7 L/kg in Beagle dogs), and a moderate to long half-life in all species (3.2 h in mice, 50.7 h in dogs) (**Table S1J; Table S1N**). The oral bioavailability of MMV688533 was >70% in rodent species (**Table S1J**). Human C_L and V_{ss} parameters calculated from rat and dog allometry were predicted to be inferior to 5% of the hepatic blood flow using two methods (see Methods section) and 5.0 L for a

70 kg patient, respectively. The predicted half-life of MMV688533 in humans was greater than 100 h (**Table S1P**).

We then predicted the efficacious single dose in humans based on: (i) the minimal parasiticidal concentration derived from PK/PD modeling of the *Pf* NOD-SCID data (**Tables S1F; S1G**); (ii) the K_{kill} derived from in vitro PRR studies (**Fig. 1B**); (iii) the PK in mouse, rat and dog used in allometric scaling (**Tables S1J-S1P**); and (iv) a biopharmaceutical model (GastroPlus®). This latter model predicted that at least 50% of a 500 mg dose was absorbed when administered in fed conditions. A 100 mg dose is absorbed up to 70% in fasted conditions while at this dose, the food effect is less than 30% (data not shown). Using these parameters, a single oral administration of 30 mg MMV688533 in humans was predicted to maintain its concentration above the minimal parasiticidal concentration over a period of 96 h, which covers two *P. falciparum* erythrocytic replication cycles, and to reduce parasitemia by at least 6 logs when a conservative in vitro log PRR value was capped at 3. Similarly, a dose of 24 mg was predicted to reduce parasitemia when the in vitro log PRR value of 5 was used. A single-dose treatment with 66 mg of MMV688533 was predicted to reduce parasitemia by 12 logs, suggesting very favorable characteristics for future clinical studies.

MMV688533 revealed a favorable tolerability profile

In silico toxicity predictions did not raise any safety alerts other than a moderate phototoxic risk (**Table S1Q**), which proved minimal when tested in MMV688533-treated BALB/c 3T3 mouse fibroblasts exposed to UV light. Genotoxicity testing with MMV688533, including preliminary Ames and micronucleus assay were negative. Profiled on a receptor/enzyme panel, MMV688533 displayed micromolar affinity for calcium and chloride channels as well as for benzodiazepine and

dopamine receptors (**Table S1R**). Considering its similarity with cariporide, cardiovascular parameters were assessed in detail. MMV688533 had a modest effect on the hERG channel with an IC_{50} of 30 µM (data not shown) and 4.6 µM when measured by automatic and manual Patch-Clamp (**Table S1S**), respectively. Inhibition studies with Nav1.5 and Cav1.1 ion channels yielded IC_{50} values of 14 µM and 2.1 µM, respectively (**Table S1S**). When tested in the Pukinje fiber assay, MMV688533 induced mild effects that were not suggestive of a torsadogenic profile. However, because of the limited solubility of the compound in the conditions of this study, a full cardio-safety in vitro evaluation at higher concentrations was not possible. Therefore, in vivo studies were conducted to better assess potential cardiovascular safety risks. Continuous intravenous administration of MMV688533 (at 10, 20 and 30 mg/kg) to anesthetized guinea pigs did not affect blood pressure, heart rate, the ECG RR or QT intervals, or the QRS complex (data not shown). In summary, in silico, in vitro and in vivo safety studies with MMV688533 did not raise any measurable cardiotoxicity alerts.

Preliminary safety was assessed in rats and dogs via oral treatment and drug exposure measurements (Toxicokinetics: **Tables S1T, S1U**). In a non-GLP 2-week toxicity study in Sprague-Dawley rats, no clinically apparent changes were observed at 12.5, 25 and 50 mg/kg dose levels. 12.5 mg/kg/day exposure was considered the No-Observed Effect Level (NOEL) in this study due to an increase of liver biomarkers and microscopic changes (foamy macrophages, microscopic changes) at the two highest doses. In a non-GLP 2-week toxicity study in beagle dogs, (0.5 and 1 mg/kg/day once daily and 2 mg/kg/day every other day), only minimal transient changes of no safety concern were detected. In conclusion, the no-observed-adverse-effect level (NOAEL) was declared at 1 mg/kg and the corresponding cumulated exposure over 14 days was 14-fold higher than that predicted for a 30

mg single dose in humans (**Table S1V**). Such a predicted safety margin was judged promising enough to progress MMV688533 to more detailed regulatory preclinical studies before first-in-human clinical trials.

MMV688533 is maximally potent against *P. falciparum* rings and early trophozoite stages

To assess the timing of MMV688533 action, we employed an in vitro asexual blood stage susceptibility assay that measures compound activity against early and late rings, early and late trophozoites, and schizonts (*15*). The assay was validated by the stage-specific susceptibility profiles of dihydroartemisinin, chloroquine and the PI4K inhibitor KAI407 (*16*), which showed the expected peak activities on early rings, rings and trophozoites, and schizonts, respectively (*15*). MMV688533 and dihydroartemisinin shared a similar activity profile, with early rings to early trophozoites being the most susceptible, whereas schizonts were the least affected (**Fig. 2A**).

Ramping selections with *P. falciparum* asexual blood stage parasites yield low-grade resistance to MMV688533

To identify possible resistance mechanisms to the acylguanidine MMV688533, we performed single-step in vitro resistance selections by exposing triplicate flasks of 2×10^9 wild-type Dd2-B2 parasites to $3\times IC_{50}$ of MMV688533. These single-step selections did not yield resistant parasites after 60 days, suggesting a low propensity for resistance development for this compound. This was further confirmed in ramping selections, which entailed gradually increasing the drug pressure from 1 to $11\times IC_{50}$ on triplicate flasks of 2×10^8 3D7-A10 parasites each over a six-month period. This selection yielded only very low-grade resistance, with a 2 to 5-fold IC_{50} increase in each of the three drug-pressured lines (**Fig. 2B; Table 2**). Whole-genome sequencing (WGS) of four resistant clones

obtained from across the three pressured lines identified single nucleotide polymorphisms (SNPs) in five genes: a conserved *Plasmodium* protein of unknown function (PF3D7_0910300); an EH domain-containing protein (EHD; PF3D7_0304200); a conserved *Plasmodium* protein of unknown function (PF3D7_0510100); a putative RNA pseudouridylate synthase (PF3D7_0511500); and the putative ATP synthase (C/AC39) subunit (PF3D7_1464700) (**Table 2; Table S3**).

Of note, all four clones (sel. 533-CL1 – CL4, named after the last three digits of the selecting compound MMV688533 followed by the clone name), carried G98V (clones sel. 533-CL1 and sel. 533-CL4), W286R (clone sel. 533-CL2) or T92* stop codon (clone sel. 533-CL3) mutations in PF3D7_0910300, identified from three separately drug-pressured lines, suggesting a key role for this protein in conferring resistance to MMV688533. PF3D7_0910300, which we herein name *Plasmodium falciparum* acylguanidine 1 (PfACG1) in reference to the acylguanidine series, is a conserved *Plasmodium* protein of unknown function. Clone sel. 533-CL4, which also has a D218Y mutation in gene PF3D7_0304200 (PfEHD), displayed the highest level of resistance to MMV688533 (4.6-fold IC_{50} shift) (**Fig. 2B; Table 2**). This suggested an additional role for PfEHD in enhancing parasite resistance to the compound. Based on these observations, the presence of PfACG1 mutations in all the selected clones and the boost in resistance conveyed by an additional PfEHD D218Y mutation in sel. 533-CL4, we hypothesized that these two proteins, out of the five proteins identified using WGS, play a crucial role in mediating resistance to MMV688533. We chose to not assess the other three genes listed above as each harbored a mutation observed from only a single line, and unlike PF3D7_0304200 none of these three were associated with an increased degree of resistance (**Table 2**).

To test this hypothesis, we introduced the G98V and W286R mutations in PfACG1 and the D218Y mutation in PfEHD individually into wild-type 3D7-A10 parasites using a CRISPR/Cas9 gene-editing strategy. This yielded the edited lines ed. 3D7 ACG1^{G98V}, ed. 3D7 ACG1^{W286R} and ed. 3D7 EHD^{D218Y} lines respectively. The G98V mutation in the ed. 3D7 ACG1^{G98V} line conferred comparable levels of resistance to the corresponding selected clone sel. 533-CL1, whereas the W286R mutation in ed. 3D7 ACG1^{W286R} line only contributed around half of the resistance observed in sel. 533-CL2 (**Fig. 2B; Table 2)**. The D218Y mutation in PfEHD alone was insufficient to confer resistance. To test whether SNPs in PfACG1 are needed to obtain higher grade resistance to MMV688533 we introduced the D218Y mutation into the background of the clone sel. 533-CL1, using a CRISPR/Cas9 strategy. This clone harbors the G98V mutation in PfACG1. The resulting sel. ed. 533-CL1$^{EHD-D218Y}$ line showed a 6.2-fold shift in IC_{50} compared to wild-type parasites, comparable to the 4.6-fold shift in clone sel. 533-CL4. These results provide evidence that the D218Y mutation in PfEHD enhances resistance to MMV688533 only when the G98V mutation is already present in PfACG1.

Conditional knockdown of the resistance determinants PfACG1 and PfEHD does not affect in vitro parasite growth

To further explore the role of PfACG1 and PfEHD, we engineered conditional knockdown parasite lines in which we could regulate protein expression levels via the TetR-DOZI system (*17*). Normal protein levels were maintained by culturing parasites in the presence of anhydrotetracycline (aTc) (**Fig. S1A**). Western blot analysis of these lines, which harbored a C-terminal 2×HA epitope tag fused to each gene product, confirmed the expression of PfACG1 and PfEHD in the presence of aTc (**Fig. 2C; Fig. S1B)**. aTc withdrawal resulted in the loss of protein expression, confirming efficient

knockdown of the proteins. Despite the substantial knockdown observed from the Western blots, assessment of growth over two replicative cycles revealed that PfACG1 and PfEHD parasite lines, maintained in the absence of aTc, were able to progress through the intra-erythrocytic stage life cycle similar to controls, suggesting that loss of function of both proteins does not affect viability under normal culture conditions (**Fig. 2C**). To test for ex vivo compound-target interactions, we determined the IC_{50} of MMV688533 against wild-type versus knockdown conditions of PfACG1 and PfEHD. Similar to an unrelated control line, knockdown of PfACG1 and PfEHD did not result in differential susceptibility to MMV688533 (**Fig. 2D**), providing evidence that these proteins are not directly targeted by MMV688533.

MMV688533-resistant parasites do not show cross resistance to current antimalarials

To test whether resistance to MMV688533 might impact the efficacy of clinical antimalarials, we tested the 3D7 ACG1^{G98V} and 3D7 ACG1^{W286R} edited lines as well as the high-grade resistant clone sel. ed. 533-CL1$^{EHD\text{-}D218Y}$ for cross-resistance against a diverse panel of eleven known antimalarials. This study employed 72 h asexual blood stage parasite susceptibility assays across a range of drug concentrations (**Fig. 2E; Table S2**). Neither the individual G98V and W286R mutations in PfACG1 nor the multiple SNPs in sel. ed. 533-CL1$^{EHD\text{-}D218Y}$ conferred cross-resistance to these drugs, implying that MMV688533 has a novel mode of action against *P. falciparum*.

PfACG1 and PfEHD localize primarily to distinct intracellular parasite vesicles

To interrogate the subcellular localization of PfACG1 and PfEHD we performed immunofluorescence studies with a variety of cellular co-markers. We generated a doubly tagged recombinant NF54attB parasite line expressing a 3×HA tag at the C-terminus of the PfEHD

endogenous locus as well as a stably-integrated transgenic copy of PfACG1 that was C-terminally tagged with eGFP (NF54$^{3\times HA\text{-}EHD}$attB-ACG1-eGFP).

PfACG1-eGFP mainly localized to foci around the digestive vacuole (DV) of the parasite with residual labeling observed around the parasite nucleus (**Fig. 2F; Fig. S4, S6**). PfEHD likewise appeared in foci that localized mostly to the parasite periphery as well as close to the DV; other foci were also other observed, although to a lesser extent, throughout the parasite cytoplasm (**Fig. 2F; Fig. S5, S7**). Co-labeling using anti-HA and anti-GFP antibodies to assess co-localization of PfACG1 with PfEHD showed no overlap between the two fluorophores (**Fig. 2G**).

Since most of the eGFP signal for the PfACG1-fusion protein was observed adjacent to the DV we performed co-stains using antibodies directed to PfCRT, PfMDR1 or Plasmepsin II, which are known to localize to the DV (**Fig. 2H; Fig. S4A-B, S6B-C**). This confirmed proximity to the DV, but only showed infrequent, seemingly random overlap between PfACG1 and either of the DV transmembrane proteins PfCRT and PfMDR1. To investigate whether PfACG1 could overlap with neutral lipid bodies, which are often localized adjacent to the parasite DV (*18*), we carried out co-stains using LipidTOX and Nile Red (**Fig. 2I; Fig. S4C-F, S6D-G**). Although not all eGFP positive foci exclusively overlapped with these lipid bodies we observed frequent juxtaposition. These observations point to the possibility that PfACG1 partially associates with lipid storage bodies localized close to the DV. Despite our detection of an eGFP signal close to the nucleus, no overlap was detected when co-staining for the parasite endoplasmic reticulum (ER) using antibodies specific for PDI (protein disulfide isomerase; **Fig. 2J; Fig. S6H-I**). Instead, the eGFP signal showed some overlap with antibodies to ERD2 and PMT (phosphoethanolamine N-methyltransferase), which

represent markers for the cis- and trans-Golgi (*19, 20*), respectively (**Fig. 2K; Fig. S4G-J, S6J-K**). To test whether PfACG1 localized to Rab-positive vesicles that are known mediators of vesicular traffic, we co-stained with Rab5A, 5B and Rab7 antibodies. We only observed infrequent overlap, similarly to co-stains performed with antibodies against K13, a marker for hemoglobin endocytosis (*21, 22*) (**Fig. 2L; Fig. S4K-N, S6L-O**). Along these lines no colocalization was observed for PfACG1 and coronin, a protein involved in F-actin organization that has recently been associated with in vitro resistance of early ring stages to artemisinins (*23*) (**Fig. S4O**). Lastly, we assessed co-localization to the parasite mitochondrion using MitoTracker Deep Red, as well as to the apicoplast as visualized with anti-ACP antibodies. No overlap was observed between PfACG1-eGFP and those organelles (**Fig. S4P,Q**).

Similar to our observations with PfACG1, we detected PfEHD-positive foci that were close to the DV but did not co-localize with PfCRT (**Fig. 2M; Fig. S7B-C**). Co-stains using LipidTOX occasionally co-localized some of the HA-labeled PfEHD vesicles with neutral lipid bodies (**Fig. 2N; Fig. S5A-B, S7D**). To investigate PfEHD association with the parasite ER as well as the Golgi apparatus we used anti-PDI antibodies or anti-ERD2 and anti-PMT antibodies respectively. Frequent proximity and partial overlap were observed between PfEHD positive foci and the ER-resident markers PDI and BIP, whereas the Golgi stains revealed no obvious association between PfEHD and this organelle (**Fig. 2O-P; Fig. S5C-F, S7E-H**). In mammalian cells, EH domain (EHD)-containing proteins, serving as protein interaction platforms, are known to primarily function as key regulators in endocytosis (*24*). To explore whether PfEHD could play a similar role in protein and lipid trafficking processes in parasites we performed immunofluorescence (IFA) studies using antibodies to coronin and Rab proteins. We found that PfEHD vesicles that localized close to the parasite

membrane frequently overlapped with coronin, hinting at a possible interaction between the two proteins (**Fig. 2Q; Fig. S5G-J, S7I-J**). Immunofluorescence assays carried out with the panel of Rab antibodies (anti-Rab5A, 5B, 5C, Rab7 and Rab11A) as well as antibodies to K13 revealed some juxtaposition of Rab-positive vesicles and K13-positive foci with PfEHD (**Fig. S5K-P, S7K**). In contrast, when assessing potential PfEHD association with the apicoplast using anti-ACP antibodies, we did not observe overlap between the fluorophores (**Fig. S5Q**).

DISCUSSION

Here, we report an exquisitely potent antimalarial, MMV688533, discovered among Sanofi compounds active on defined human targets and that were assayed for potency against *P. falciparum* asexual blood stage parasites. Our screen of 800 compounds yielded a high hit rate, with 120 showing submicromolar antiplasmodial activity. Physicochemical analysis identified acylguanidines as the most promising series, with subsequent structure analysis relationship (SAR)-based lead optimization yielding MMV688533. Parasite reduction ratio assays revealed exceptionally fast killing, with MMV688533 reducing the parasite load by >3 log within 24 h after drug addition, similar to dihydroartemisinin and considerably faster than the comparator first-line drugs chloroquine and pyrimethamine. MMV688533 also displayed minimal toxicity against mammalian cells, slow clearance, and a long half-life predicted at 100 h in humans. Single-dose efficacy in the *P. falciparum*-infected SCID mouse model was excellent, with parasite clearance and delayed recrudescence observed at doses as low as 5 mg/kg. These data highlight the therapeutic potential of this novel class of antimalarials.

Whole-cell screens for antimalarials have in recent years yielded multiple potent antimalarials that despite their promise have encountered parasite resistance at frequencies and levels that pose an important concern for their further development as curative drugs (*25*). For example, inhibitors of the drug targets PfATP4 or PfeEF2 can select for resistance from as a few as 10^6-10^7 parasites, with SNPs causing IC_{50} increases of up to several hundred-fold ((*26*-*28*); unpublished results). In contrast, using these same selection procedures (*29*), MMV688533 yielded no resistance when used to pressure even large parasite inocula (6×10^9). Low-grade resistance could only be achieved using a ramping method of gradually increasing drug concentrations over a 6-month period. Parasite clones from these selections showed 2- to 5-fold higher IC_{50} values against MMV688533. Whole-genome sequencing identified two distinct point mutations or a stop codon in the PfACG1 gene in all clones assayed from three independent selections. Upon gene editing, both point mutations afforded only a 2-fold IC_{50} increase. One clone also harbored a point mutation in PfEHD, which upon editing into a PfACG1 mutant line resulted in a 6-fold higher IC_{50} relative to the drug-sensitive 3D7 line. Other editing results showed that this PfEHD mutation on its own was insufficient to mediate parasite resistance. We note that three other genes were observed to each harbor a single non-synonymous mutation. These mutations occurred separately in only one of the three flasks and may be attributable to stochastic events that arise naturally at low frequency during extended in vitro culture (*30, 31*).

PfACG1 and PfEHD are both considered to be dispensable for *P. falciparum* asexual blood stage growth in vitro (*32*), consistent with our cKD data in which no evident growth inhibition occurred despite virtually complete protein knockdown (**Fig. 2C**). PfACG1, previously annotated as a conserved protein of unknown function, is only conserved among Apicomplexan parasites of the genus *Plasmodium*, with minimal (~ 20%) amino acid identity to *Cryptotosporidium andersoni* and

372 *C. muris*. Protein sequence analysis shows a signal peptide at the N-terminus and a single
373 transmembrane domain at the C-terminal end. Little else is known about this protein. PfEHD
374 contains a highly-conserved Eps15 homology domain (EHD) involved in protein-protein interactions
375 and found in proteins that play a key role in endocytosis (*24*). PfEHD has previously been linked to
376 vesicular trafficking in *P. falciparum* parasites (*33*).
377
378 PfACG1 and PfEHD did not co-localize in our immunofluorescence assays. Nonetheless, PfACG1
379 co-localized with the neutral lipid markers LipidTOX and Nile Red, as well as the Golgi markers
380 ERD2 that mediates protein retention in the ER and PMT that plays a critical role in
381 phosphatidylcholine synthesis, suggesting its role in vesicular trafficking or storage of lipids. In
382 contrast, PfEHD showed some co-localization with the ER markers ERD2 and PDI as well as the
383 actin-binding protein coronin. PfEHD has previously been shown to be an interacting partner of AP-
384 2μ, an adapter protein that is essential for endocytosis and intracellular trafficking (*34*). Taken
385 together, these data suggest that PfACG1 and PfEHD might be involved in related intracellular
386 trafficking pathway(s) acted upon by MMV688533, which would be consistent with our observation
387 that mutations in both proteins contributed to resistance to this compound. These results, along with
388 lack of chemical-genetic interaction observed using the cKD lines (**Fig. 2C**), suggest that neither of
389 these two proteins is the actual target and function instead as resistance mediators. These data suggest
390 that MMV688533's mode of action involves inhibition of vesicular trafficking and/or lipid storage
391 pathways. At present this compound can be considered "target-less", a feature shared by many
392 antimalarials in clinical use or advanced stages of development, including lumefantrine, quinine,
393 artemisinin derivatives, OZ439, and KAF156 (*25, 35*). Further studies are clearly required to define
394 the mode of action of MMV688533.

In conclusion, we report the novel acylguanidine MMV688533 with favorable fast-acting and long-lasting pharmacokinetic/pharmacodynamic properties. Drug selection studies showed that parasites could only acquire low-grade resistance with large inocula, and no cross-resistance was observed with established antimalarials or advanced preclinical candidates. These data suggest a novel mode of action for MMV688533, which appears to involve lipid-associated intracellular trafficking of essential components. The promising preclinical therapeutic margin and very low single doses predicted to be efficacious in humans should improve compliance and enable a low cost of goods. Further safety and pharmacological preclinical evaluations are currently ongoing to support the initiation of human clinical trials.

MATERIALS AND METHODS

Study design

This study's objective was to harness the potential of compounds with known drug-like properties, which had been successful in fueling discovery and development pipelines in several therapeutic areas, as a source of potential antimalarial candidates with novel modes of actions. Screening against *P. falciparum* asexual blood stage parasites led us to identify an acylguanidine chemical series with good potency and physicochemical properties. Medicinal chemistry yielded analogs with improved parasite selectivity and pharmacokinetic properties. Prioritized compounds were assayed for in vivo efficacy in a humanized mouse model of *P. falciparum* infection. Preclinical toxicity studies with 4- or14-day exposures were then performed in rats and dogs to predict a safety margin for clinical use. Cross-resistance and drug selection studies were used to test for resistance liabilities. Conditional knockdown and gene editing experiments, along with immunofluorescence

imaging, were leveraged to explore compound mode of action. All assays were performed with multiple repeats with technical duplicates or triplicates, with positive and negative controls, as indicated in the Materials and Methods and in Figure legends.

MMV688533 synthesis

MMV688533 was synthesized as described in the Supplementary Materials and Methods and illustrated in **Fig. S8**.

Compound potency against *P. falciparum* and *P. vivax* parasites

Antimalarial activity against resistant culture-adapted strains of *P. falciparum* and clinical field isolates was performed with the modified [^{3}H]-hypoxanthine incorporation assay, as previously reported (*36*). Ex vivo potency against *P. falciparum* and *P. vivax* clinical isolates was determined as described in the Supplementary Materials and Methods.

Determination of the in vitro rate of killing (parasite reduction ratio, PRR)

As described in (*12*), the compound IC_{50} was determined via [^{3}H]-hypoxanthine incorporation. For PRR assays, 10^5 3D7A parasites cultures were exposed to MMV688533 at $10\times IC_{50}$ for 120 h. Drug treatment was renewed every 24 h over the entire period. Parasite aliquots were taken from the treated cultures every 24 h, with drug washout, throughout the 5-day treatment period. Fresh RBC and new media were then added to the drug-free parasites, which were serially diluted in quadruplicate into 96 well plates. Growth in individual wells was detected after 3 and 4 weeks using [^{3}H]-hypoxanthine incorporation. The number of viable parasites was determined by the dilution down to which growth

was observed. The rate of killing was represented by the log of viable parasites as a function of treatment duration. PRR was defined as the log-linear reduction of viable parasites over 48 h.

Determination of efficacy and pharmacokinetic profiles in the Pf SCID mouse model

Assays used the *P. falciparum* Pf3D70087/N9 line (*14*), which was propagated in 23-28 gram female NOD-scid IL-2Rγnull mice (NSG) (Charles River, France) or NOG-scid IL-2Rγnull mice (NOG) (Taconic, Denmark) at The Art of Discovery (TAD). In vivo efficacy trials are described in the Supplementary Materials and Methods.

Parasite stage-specificity assays

In vitro IC_{50} values were determined by incubating parasites for 72 h across a range of 10 different concentrations of antimalarial compounds plus two no-compound controls. Stage-specificity assays used a modified protocol with tightly-synchronized parasites tested at different starting stages of the ABS cycle (*15*).

P. falciparum resistance selections

Single-step selections for MMV688533 resistance employed triplicate flasks of 2×10^9 Dd2-B2 parasites exposed to 5-14× the IC_{50} (25–80 nM) of MMV688533. Selections were terminated after 60 days as resistant parasites had not emerged. Ramping selections used triplicate flasks of 2×10^8 3D7-A10 parasites exposed to MMV688533 at concentrations that increased gradually from 1-10× the IC_{50} (5.5–60 nM) over a six-month period. Resistant clones were obtained from the bulk cultures of the ramping selections by limiting dilution, and four clones were selected for whole-genome sequencing. MMV688533 growth inhibition was determined by staining the parasites with SYBR

Green and MitoTracker Deep Red (Life Technologies) followed by flow cytometry (Accuri C6, BD Biosciences) (*37*). IC_{50} values were derived from growth inhibition data using nonlinear regression (Prism 9.0, GraphPad). Unless stated otherwise, all drug assays were performed on at least four separate occasions (as biological repeats) with two technical replicates.

Whole-genome sequencing analysis and genome editing

The 3D7-A10 parent and MMV688533-resistant clones were subjected to whole-genome sequencing using an Illumina TruSeq DNA PCR-Free library preparation protocol and a MiSeq sequencing platform, as described (*38*). CRISPR/Cas9 and mycobacteriophage Bxb1 serine integrase system-based gene editing, including cKDs, is detailed in the Supplementary Materials and Methods.

Immunofluorescence assays

Protein localization assays were performed as described (*22*), (Supplementary Materials and Methods).

Statistical analysis

Mann-Whitney *U* tests were performed (using Prism 9.0; GraphPad) to test for statistical significance between isogenic parasite lines in their drug IC_{50} values (**Fig. 2B; Table S2**). Wilcoxon rank sum tests were used to identify significant differences in drug susceptibility between *P. falciparum* field isolates (**Table 1**).

SUPPLEMENTARY MATERIALS

Table S1H. MMV688533 in vitro metabolic clearances in microsomes and hepatocytes from different species

Table S1I. MMV688533 inhibition of cytochromes P450 (CYP)

Table S1J. MMV688533 pharmacokinetic parameters in male Swiss mice and male Sprague Dawley rats after intravenous and oral route administration

Table S1K. MMV688533 pharmacokinetic parameters in male Sprague Dawley rats after oral administration

Table S1L. MMV688533 blood toxicokinetic parameters in male and female Sprague Dawley rats

Table S1M. MMV688533 mean biliary and urinary excretion parameters in male Sprague Dawley rats

Table S1N. MMV688533 mean pharmacokinetic parameters in female Beagle dogs after intravenous injection

Table S1O. Mean blood pharmacokinetic parameters of MMV688533 and its metabolite RA14677213 following a single oral administration as capsule or oral solution to pentagastrin-induced male Beagle dogs

Table S1P. MMV688533 predicted human parameters

Table S1Q. MMV688533 *in silico* prediction of genotoxicity/organ toxicity

Table S1R. MMV688533 off-target activities

Table S1S. MMV688533 in vitro activity in µM on different cardiac ion channels

Table S1T. MMV688533 non-compartmental analysis of exposure in male Sprague Dawley rats

Table S1U. MMV688533 cumulated exposure over 14 days of treatment in Beagle dogs

Table S1V. Calculation of MMV688533 safety margin based on cumulative AUC over 14 days at the NOAEL dose in rats and dogs

Table S2. Asexual blood stage IC_{50} data in nM of MMV688533-resistant parasite lines against common antimalarials

Table S3. Protein functional pathway relationships

References (*39-67*)

ACKNOWLEDGEMENTS

We thank Drs. Didier Leboulleux (Sanofi, now Evotec) and Antonio Laso and Eneko Ochoa from AleoVitro SL for their kind contribution to this study. We thank Dr. Jeya Prakash (Syngene) for the synthesis of the compounds, and Christian Scheurer, Sibylle Sax and Christoph Fischli (Swiss TPH) for the generation of in vitro parasitology data. We are grateful to Drs. Koen Dechering (TropIQ Health Sciences) and Michael Delves (London School of Hygiene & Tropical Medicine) for providing *P. falciparum* liver and sexual stage data, respectively. We also thank MMV colleagues for their critical review of the manuscript. **Funding:** Funding for this work was provided by the Medicines for Malaria Venture and in-kind contribution from Sanofi. D.A.F. gratefully acknowledges funding support from the NIH (R01 AI124678, R01 AI109023), the Bill & Melinda Gates Foundation (OPP1201387) and the Department of Defense (W81XWH-19-1-0086). S.M. is grateful for support from a Human Frontier Science Program Long-term Postdoctoral Fellowship LT000976/2016-L. **Author contributions:** J.M.M., C.P., I.A.-B., G.C., L.F., A.P., D.A.F. and D.L. designed the study; J.M.M., J.B., N.F.G., C.F.A.P., K.R., P.D., M.B.J.-D., J.M., G.W., R.N. and P.T. generated data; J.M.M., C.P., J.B., X.B., N.F.G., C.F.A.P., K.R., T.Y., S.M., S.K., P.D., M.B.J.-D., J.M., D.B., M.C., N.G., S.W., R.N.P., G.W., R.N., P.T., R.A.C., P.J.R., L.M.S., F.J.G., J.M.A., E.G., T.B., T.V., G.T., J.-M.G., M.F.N., N.B., I.A.-B., F.E., D.A.F. and D.L. analyzed data; C.P., X.B., A.-C.U., R.A.C., J.J., S.S., S.B., J.M., L.S., G.L., M.-J.C., I.A.-B., B.B. and J.C.N. provided reagents

or expertise; M.R., M.D., R.M., L.B., B.B., S.C., G.C., L.F., A.P., D.A.F. and D.L. were the project managers; J.M.M., D.A.F. and D.L. wrote the manuscript, with input from all the authors. **Competing interests:** M.R., M.C., N.G., D.B., L.B., F.E., B.B., S.C., and D.L. are employees of MMV. C.P., X.B., P.D., S.K., J.M.A., E.G., T.B., T.V., G.T., J.-M.G., J.M., L.S., G.L., M.-J.C., M.F.N., M.D., R.M., N.B., L.F., and A.P. are employees of Sanofi. M.B.J.-D., L.M.S., and F.J.G., are employees of GSK. J.J., S.S., and S.B. are employees of Syngene. G.C. is an employee of Bioaster. All other authors declare no competing interests. C.P. A.P. G.C., and S.C. are authors on the MMV688533 patent WO2019008027A1 (PCT/EP2018/068079). **Data and materials availability:** All data associated with this study are present in the paper and/or the Supplementary Materials.

564 **Table 1.** MMV688533 activity against Plasmodium parasite lines and field isolates.

	Laboratory lines	Laboratory lines	Laboratory lines	Laboratory lines	Clinical field isolates (Uganda)	Clinical field isolates (Papua, Indonesia)	Clinical field isolates (Papua, Indonesia)
	P. falciparum	*P. falciparum*	*P. falciparum*	*P. falciparum*	*P. falciparum*	*P. falciparum*	*P. vivax*
Antimalarial	3D7 (Median, N)	Dd2 (Median, N)	FC27 (Mean, N)	K1 (Mean, N)	Median (N; range)	Median (N; range)	Median (N; range)
MMV688533	1.9 (4)	3.0 (4)	9.7 (2)	19 (2)	1.3 (143; 0.02 - 6.3)	18.9 (15; 5.3-39.2)	12.0 (6; 5.4-19.9)
Chloroquine	11 (11)	347 (10)	10.9 (2)	100.3 (2)	17*** (143; 2.1 - 346)	64.8*** (15; 38.3-283)	36.4* (6; 11.6-114)
Piperaquine	4.4 (11)	7.9 (10)	25.8 (2)	111.2 (2)	5.1*** (140; 0.3 - 26)	60.8*** (15; 17.6-130)	46.6* (6; 15.0-135)
Mefloquine	4.8 (11)	6.6 (10)	37.2 (2)	8 (2)	8.3*** (120; 0.5 - 24)	10.0 (15; 4.9-41.9)	11.2 (6; 8.1-20.7)
DHA/artesunate[a]	1.9 (9)	1.7 (9)	0.6 (2)	1.1 (2)	1.5 (142; 0.1 - 9.0)	1.2*** (15; 0.4-4.3)	0.6* (6; 0.3-2.4)

565 In vitro activity against *Plasmodium* culture-adapted lines or field isolates was calculated from dose-response curves and is shown as
566 median or mean half-maximal growth inhibition concentrations (IC_{50} values) in nM. For the laboratory lines, numbers of independent
567 repeats are shown in brackets. 3D7 and FC27 are chloroquine-sensitive whereas Dd2 and K1 are chloroquine-resistant. Potency of the
568 other antimalarials was compared to MMV688533 using a Wilcoxon rank sum test. *$p<0.05$; ***$p<0.001$. [a]DHA was tested on 3D7,
569 Dd2 and Ugandan parasites, whereas artesunate was tested on FC27, K1 and Papua/Indonesian parasites.

570

Table 2. Mutations identified in MMV688533-selected resistant *P. falciparum* clones and validated using CRISPR/Cas9 gene editing.

Gene product	Gene ID	Amino acid substitution							
		sel. 533-CL2	ed. 3D7 ACG1^{W286R}	sel. 533-CL3	sel. 533-CL4	ed. 3D7 ACG1^{G98V}	ed. 3D7 EHD^{D218Y}	sel. 533-CL1	sel. ed. 533-CL1$^{EHD-D218Y}$
		3.1× IC_{50}	1.7× IC_{50}	2.5× IC_{50}	4.6× IC_{50}	1.8× IC_{50}	1.2× IC_{50}	2.2× IC_{50}	6.2× IC_{50}
Conserved *Plasmodium* protein (PfACG1)	PF3D7_0910300	W286R	W286R	T92*	G98V	G98V	wt	G98V	G98V
EH domain-containing protein (PfEHD)	PF3D7_0304200	wt	wt	wt	D218Y	wt	D218Y	wt wt	D218Y
Conserved *Plasmodium* protein	PF3D7_0510100	wt	wt	wt	wt	wt	wt	N1042H	N1042H
RNA pseudouridylate synthase, putative	PF3D7_0511500	wt	wt	K2762E	wt	wt	wt	wt	wt
ATP synthase (C/AC39, subunit, putative	PF3D7_1464700	L260I	wt	wt	wt	wt	wt	wt	wt

Four parasite clones (sel. 533-CL1 from flask 1, sel. 533-CL2 and 533-CL3 from flask 2, and sel. 533-CL4 from flask 3) were generated from selections (sel.), and named after the last 3 digits of the selecting compound (MMV688533) followed by the clone number. These clones were then chosen for whole-genome sequencing. Fold IC_{50} increases compared to the parent 3D7-A10 are indicated below the clone names. *P. falciparum* ACG1^{W286R}, ACG1^{G98V} and EHD^{D218Y} strains were gene edited (ed.) using CRISPR/Cas9 to introduce the designated mutation into 3D7-A10 parasites. The sel. ed. 533-CL1$^{EHD-D218Y}$ clone was generated by CRISPR/Cas9 editing the EHD ^{D218Y} mutation into the selected 533-CL1 clone. wt: wild-type, *: stop mutation resulting from a deletion-induced frameshift.

FIGURE LEGENDS

Fig. 1. The preclinical antimalarial candidate MMV688533 has a fast rate of antiplasmodial activity that offers potent single-dose activity against *P. falciparum* infection in a humanized mouse model. (A) Structural representation showing the optimization of the acylguanidine series from the initial hit MMV668603 and the lead MMV669851 to the candidate MMV688533. **(B)** Mean ± SD values of viable *P. falciparum* parasites determined daily for 5 days after in vitro incubation with MMV688533 at 10× the IC_{50}. Dihydroartemisinin, Chloroquine, pyrimethamine and atovaquone were included as reference antimalarial drugs. **(C)** Mean ± SD values of *P. falciparum* viability determined daily for 5 days following MMV688533 treatment at doses corresponding to 1×, 3×, 10× or 30× the IC_{50}. **(D)** Compound efficacy was assessed by measuring the initial clearance and time of recrudescence of *P. falciparum* in the peripheral blood of humanized mice administered single doses of MMV688533 ranging from 0.5 mg/kg to 75 mg/kg (two mice per dose). DHA (50 mg/kg) and vehicle were included as controls. **(E)** Concentration of MMV688533 in serial blood samples obtained after administering different doses to *P. falciparum*-infected humanized mice assayed in (D). LOQ: Limit Of Quantification.

Fig. 2. MMV688533 antiplasmodial activity is unrelated to existing antimalarials and selects for low-grade resistance mediated in part by mutations in PfACG1 and PfEHD. (A) In vitro asexual blood stage susceptibility assay showing MMV688533 activity in early and late rings, early and late trophozoites, and schizonts. IC_{50} values are shown as means ± SEM (N>3, n = 2). **(B)** Mean ± SEM IC_{50} values of selected (sel.) (533-CL1, 533-CL2 and 533-CL4), edited (ed.) ($PfACG1^{G98V}$, $PfACG1^{W286R}$, $PfEHD^{D218Y}$) lines and the sel. ed. line 533-$CL1^{EHD\text{-}D218Y}$ compared to the 3D7-A10 parental line. N>6, n = 2; $^{**}P$ <0.01, $^{***}P$ <0.0005; ns: not significant. **(C)** Western blot data

showing effective reduction in PfACG1 and PfEHD protein levels upon removal of aTc, as detected using antibodies specific to the 2×HA tag added to the C-terminus of each protein. Parasite survival was measured by quantifying expression of the integrated RLuc cassette (**Fig. S1**), in the presence (50 nM) or absence of aTc. Data represent the mean of three biological replicates and are normalized to a fully inhibitory concentration of chloroquine (200 nM). **(D)** Dose-response curves for MMV688533 against PfACG1 and PfEHD conditional knock-down (ckD) parasites expressing wild-type or substantially reduced levels of each protein upon culturing with 500 nM aTc or no aTc, respectively. **(E)** G98V and W286R mutations in PfACG1 and a combination of both G98V in PfACG1 and D218Y in PfEHD in sel. ed. 533-CL1$^{EHD\text{-}D218Y}$ did not confer cross-resistance to a panel of known antimalarial drugs compared to the 3D7-A10 parent. Mean ± SEM; N>3, n = 2. **(F)** Fluorescence microscopy images of fixed NF54$^{3\times HA\text{-}EHD}$attB-ACG1-eGFP parasites either stained with anti-GFP (green) antibodies or anti-HA (magenta) antibodies. Nuclei were stained with DAPI (blue). Scale bars: 2 µm. **(G)** Fluorescence microscopy image of fixed and doubly stained NF54$^{3\times HA\text{-}EHD}$attB-ACG1-eGFP parasites using anti-GFP (green) and anti-HA (magenta) antibodies. Nuclei were stained with DAPI (blue). Scale bars: 2 µm. **(H-L)** Fluorescence microscopy images and 3D reconstructions of fixed NF54$^{3\times HA\text{-}EHD}$attB-ACG1-eGFP parasites co-stained with antibodies to anti-GFP (green) and **(H)** anti-PfCRT antibodies, **(I)** LipidTOX neutral lipid stain, **(J)** anti-PDI, **(K)** anti-ERD2 or **(L)** anti-Rab5A (red) antibodies. Nuclei were stained with DAPI (blue). Scale bars: 2 µm. **(M-Q)** Fluorescence microscopy images and 3D reconstructions of fixed NF54$^{3\times HA\text{-}EHD}$attB-ACG1-eGFP parasites co-stained with antibodies to anti-HA (magenta) and **(M)** anti-PFCRT antibodies, **(N)** LipidTOX neutral lipid stain, **(O)** anti-PDI, **(P)** anti-ERD2 or **(Q)** anti-coronin (cyan) antibodies. Nuclei were stained with DAPI (blue). Scale bars: 2 µm.

REFERENCES

1. World Health Organization. World malaria report 2020. https://www.who.int/teams/global-malaria-programme/reports/world-malaria-report-2020 (2019).
2. M. D. Conrad, P. J. Rosenthal, Antimalarial drug resistance in Africa: the calm before the storm? *Lancet Infect. Dis.* **19**, e338-e351 (2019).
3. M. Imwong, M. Dhorda, K. Myo Tun, A. M. Thu, A. P. Phyo, S. Proux, K. Suwannasin, C. Kunasol, S. Srisutham, J. Duanguppama, R. Vongpromek, C. Promnarate, A. Saejeng, N. Khantikul, R. Sugaram, S. Thanapongpichat, N. Sawangjaroen, K. Sutawong, K. T. Han, Y. Htut, K. Linn, A. A. Win, T. M. Hlaing, R. W. van der Pluijm, M. Mayxay, T. Pongvongsa, K. Phommasone, R. Tripura, T. J. Peto, L. von Seidlein, C. Nguon, D. Lek, X. H. S. Chan, H. Rekol, R. Leang, C. Huch, D. P. Kwiatkowski, O. Miotto, E. A. Ashley, M. P. Kyaw, S. Pukrittayakamee, N. P. J. Day, A. M. Dondorp, F. M. Smithuis, F. H. Nosten, N. J. White, Molecular epidemiology of resistance to antimalarial drugs in the Greater Mekong subregion: an observational study. *Lancet Infect. Dis.* **20**, 1470-1480 (2020).
4. A. Uwimana, E. Legrand, B. H. Stokes, J. M. Ndikumana, M. Warsame, N. Umulisa, D. Ngamije, T. Munyaneza, J. B. Mazarati, K. Munguti, P. Campagne, A. Criscuolo, F. Ariey, M. Murindahabi, P. Ringwald, D. A. Fidock, A. Mbituyumuremyi, D. Menard, Emergence and clonal expansion of in vitro artemisinin-resistant *Plasmodium falciparum* kelch13 R561H mutant parasites in Rwanda. *Nat. Med.* **26**, 1602-1608 (2020).
5. M. A. Phillips, J. N. Burrows, C. Manyando, R. H. van Huijsduijnen, W. C. Van Voorhis, T. N. C. Wells, Malaria. *Nat. Rev. Dis. Primers* **3**, 17050 (2017).
6. D. Plouffe, A. Brinker, C. McNamara, K. Henson, N. Kato, K. Kuhen, A. Nagle, F. Adrian, J. T. Matzen, P. Anderson, T. G. Nam, N. S. Gray, A. Chatterjee, J. Janes, S. F. Yan, R. Trager, J. S. Caldwell, P. G. Schultz, Y. Zhou, E. A. Winzeler, In silico activity profiling reveals the mechanism of action of antimalarials discovered in a high-throughput screen. *Proc. Natl. Acad. Sci. USA* **105**, 9059-9064 (2008).
7. F. J. Gamo, L. M. Sanz, J. Vidal, C. de Cozar, E. Alvarez, J. L. Lavandera, D. E. Vanderwall, D. V. Green, V. Kumar, S. Hasan, J. R. Brown, C. E. Peishoff, L. R. Cardon,

J. F. Garcia-Bustos, Thousands of chemical starting points for antimalarial lead identification. *Nature* **465**, 305-310 (2010).

8. W. A. Guiguemde, A. A. Shelat, D. Bouck, S. Duffy, G. J. Crowther, P. H. Davis, D. C. Smithson, M. Connelly, J. Clark, F. Zhu, M. B. Jimenez-Diaz, M. S. Martinez, E. B. Wilson, A. K. Tripathi, J. Gut, E. R. Sharlow, I. Bathurst, F. El Mazouni, J. W. Fowble, I. Forquer, P. L. McGinley, S. Castro, I. Angulo-Barturen, S. Ferrer, P. J. Rosenthal, J. L. Derisi, D. J. Sullivan, J. S. Lazo, D. S. Roos, M. K. Riscoe, M. A. Phillips, P. K. Rathod, W. C. Van Voorhis, V. M. Avery, R. K. Guy, Chemical genetics of *Plasmodium falciparum*. *Nature* **465**, 311-315 (2010).

9. K. Katsuno, J. N. Burrows, K. Duncan, R. Hooft van Huijsduijnen, T. Kaneko, K. Kita, C. E. Mowbray, D. Schmatz, P. Warner, B. T. Slingsby, Hit and lead criteria in drug discovery for infectious diseases of the developing world. *Nat Rev Drug Discov* **14**, 751-758 (2015).

10. H. J. Rupprecht, J. vom Dahl, W. Terres, K. M. Seyfarth, G. Richardt, H. P. Schultheibeta, M. Buerke, F. H. Sheehan, H. Drexler, Cardioprotective effects of the Na(+)/H(+) exchange inhibitor cariporide in patients with acute anterior myocardial infarction undergoing direct PTCA. *Circulation* **101**, 2902-2908 (2000).

11. Q. Chen, Y. Liu, X. L. Zhu, F. Feng, H. Yang, W. Xu, Increased NHE1 expression is targeted by specific inhibitor cariporide to sensitize resistant breast cancer cells to doxorubicin in vitro and in vivo. *BMC Cancer* **19**, 211 (2019).

12. L. M. Sanz, B. Crespo, C. De-Cozar, X. C. Ding, J. L. Llergo, J. N. Burrows, J. F. Garcia-Bustos, F. J. Gamo, *P. falciparum* in vitro *k*illing rates allow to discriminate between different antimalarial mode-of-action. *PLoS One* **7**, e30949 (2012).

13. N. J. White, Qinghaosu (artemisinin): the price of success. *Science* **320**, 330-334 (2008).

14. I. Angulo-Barturen, M. B. Jimenez-Diaz, T. Mulet, J. Rullas, E. Herreros, S. Ferrer, E. Jimenez, A. Mendoza, J. Regadera, P. J. Rosenthal, I. Bathurst, D. L. Pompliano, F. Gomez de las Heras, D. Gargallo-Viola, A murine model of falciparum-malaria by in vivo selection of competent strains in non-myelodepleted mice engrafted with human erythrocytes. *PLoS One* **3**, e2252 (2008).

15. J. M. Murithi, E. S. Owen, E. S. Istvan, M. C. S. Lee, S. Ottilie, K. Chibale, D. E. Goldberg, E. A. Winzeler, M. Llinas, D. A. Fidock, M. Vanaerschot, Combining stage specificity and

metabolomic profiling to advance antimalarial drug discovery. *Cell Chem. Biol.* **27**, 158-171 e153 (2020).

16. C. W. McNamara, M. C. Lee, C. S. Lim, S. H. Lim, J. Roland, O. Simon, B. K. Yeung, A. K. Chatterjee, S. L. McCormack, M. J. Manary, A. M. Zeeman, K. J. Dechering, T. S. Kumar, P. P. Henrich, K. Gagaring, M. Ibanez, N. Kato, K. L. Kuhen, C. Fischli, A. Nagle, M. Rottmann, D. M. Plouffe, B. Bursulaya, S. Meister, L. Rameh, J. Trappe, D. Haasen, M. Timmerman, R. W. Sauerwein, R. Suwanarusk, B. Russell, L. Renia, F. Nosten, D. C. Tully, C. H. Kocken, R. J. Glynne, C. Bodenreider, D. A. Fidock, T. T. Diagana, E. A. Winzeler, Targeting *Plasmodium* PI(4)K to eliminate malaria. *Nature* **504**, 248-253 (2013).

17. S. M. Ganesan, A. Falla, S. J. Goldfless, A. S. Nasamu, J. C. Niles, Synthetic RNA-protein modules integrated with native translation mechanisms to control gene expression in malaria parasites. *Nat. Commun.* **7**, 10727 (2016).

18. K. E. Jackson, N. Klonis, D. J. Ferguson, A. Adisa, C. Dogovski, L. Tilley, Food vacuole-associated lipid bodies and heterogeneous lipid environments in the malaria parasite, *Plasmodium falciparum*. *Mol. Microbiol.* **54**, 109-122 (2004).

19. H. G. Elmendorf, K. Haldar, Identification and localization of ERD2 in the malaria parasite *Plasmodium falciparum*: separation from sites of sphingomyelin synthesis and implications for organization of the Golgi. *EMBO J.* **12**, 4763-4773 (1993).

20. W. H. Witola, G. Pessi, K. El Bissati, J. M. Reynolds, C. B. Mamoun, Localization of the phosphoethanolamine methyltransferase of the human malaria parasite *Plasmodium falciparum* to the Golgi apparatus. *J. Biol. Chem.* **281**, 21305-21311 (2006).

21. J. Birnbaum, S. Scharf, S. Schmidt, E. Jonscher, W. A. M. Hoeijmakers, S. Flemming, C. G. Toenhake, M. Schmitt, R. Sabitzki, B. Bergmann, U. Frohlke, P. Mesen-Ramirez, A. Blancke Soares, H. Herrmann, R. Bartfai, T. Spielmann, A Kelch13-defined endocytosis pathway mediates artemisinin resistance in malaria parasites. *Science* **367**, 51-59 (2020).

22. N. F. Gnadig, B. H. Stokes, R. L. Edwards, G. F. Kalantarov, K. C. Heimsch, M. Kuderjavy, A. Crane, M. C. S. Lee, J. Straimer, K. Becker, I. N. Trakht, A. R. Odom John, S. Mok, D. A. Fidock, Insights into the intracellular localization, protein associations and artemisinin resistance properties of *Plasmodium falciparum* K13. *PLoS Pathog.* **16**, e1008482 (2020).

714 23. A. R. Demas, A. I. Sharma, W. Wong, A. M. Early, S. Redmond, S. Bopp, D. E. Neafsey,
715 S. K. Volkman, D. L. Hartl, D. F. Wirth, Mutations in *Plasmodium falciparum* actin-
716 binding protein coronin confer reduced artemisinin susceptibility. *Proc. Natl. Acad. Sci.*
717 *USA* **115**, 12799-12804 (2018).
718 24. N. B. Miliaras, B. Wendland, EH proteins: multivalent regulators of endocytosis (and other
719 pathways). *Cell Biochem. Biophys.* **41**, 295-318 (2004).
720 25. B. Blasco, D. Leroy, D. A. Fidock, Antimalarial drug resistance: linking *Plasmodium*
721 *falciparum* parasite biology to the clinic. *Nat. Med.* **23**, 917-928 (2017).
722 26. M. Rottmann, C. McNamara, B. K. Yeung, M. C. Lee, B. Zou, B. Russell, P. Seitz, D. M.
723 Plouffe, N. V. Dharia, J. Tan, S. B. Cohen, K. R. Spencer, G. E. Gonzalez-Paez, S. B.
724 Lakshminarayana, A. Goh, R. Suwanarusk, T. Jegla, E. K. Schmitt, H. P. Beck, R. Brun,
725 F. Nosten, L. Renia, V. Dartois, T. H. Keller, D. A. Fidock, E. A. Winzeler, T. T. Diagana,
726 Spiroindolones, a potent compound class for the treatment of malaria. *Science* **329**, 1175-
727 1180 (2010).
728 27. B. Baragana, I. Hallyburton, M. C. Lee, N. R. Norcross, R. Grimaldi, T. D. Otto, W. R.
729 Proto, A. M. Blagborough, S. Meister, G. Wirjanata, A. Ruecker, L. M. Upton, T. S.
730 Abraham, M. J. Almeida, A. Pradhan, A. Porzelle, T. Luksch, M. S. Martinez, T. Luksch,
731 J. M. Bolscher, A. Woodland, S. Norval, F. Zuccotto, J. Thomas, F. Simeons, L.
732 Stojanovski, M. Osuna-Cabello, P. M. Brock, T. S. Churcher, K. A. Sala, S. E. Zakutansky,
733 M. B. Jimenez-Diaz, L. M. Sanz, J. Riley, R. Basak, M. Campbell, V. M. Avery, R. W.
734 Sauerwein, K. J. Dechering, R. Noviyanti, B. Campo, J. A. Frearson, I. Angulo-Barturen,
735 S. Ferrer-Bazaga, F. J. Gamo, P. G. Wyatt, D. Leroy, P. Siegl, M. J. Delves, D. E. Kyle, S.
736 Wittlin, J. Marfurt, R. N. Price, R. E. Sinden, E. A. Winzeler, S. A. Charman, L. Bebrevska,
737 D. W. Gray, S. Campbell, A. H. Fairlamb, P. A. Willis, J. C. Rayner, D. A. Fidock, K. D.
738 Read, I. H. Gilbert, A novel multiple-stage antimalarial agent that inhibits protein
739 synthesis. *Nature* **522**, 315-320 (2015).
740 28. A. H. Lee, D. A. Fidock, Evidence of a mild mutator phenotype in Cambodian *Plasmodium*
741 *falciparum* malaria parasites. *PLoS One* **11**, e0154166 (2016).
742 29. X. C. Ding, D. Ubben, T. N. Wells, A framework for assessing the risk of resistance for
743 anti-malarials in development. *Malar. J.* **11**, 292 (2012).

744 30. S. E. Bopp, M. J. Manary, A. T. Bright, G. L. Johnston, N. V. Dharia, F. L. Luna, S.
745 McCormack, D. Plouffe, C. W. McNamara, J. R. Walker, D. A. Fidock, E. L. Denchi, E.
746 A. Winzeler, Mitotic evolution of *Plasmodium falciparum* shows a stable core genome but
747 recombination in antigen families. *PLoS Genet.* **9**, e1003293 (2013).
748 31. A. Claessens, W. L. Hamilton, M. Kekre, T. D. Otto, A. Faizullabhoy, J. C. Rayner, D.
749 Kwiatkowski, Generation of antigenic diversity in *Plasmodium falciparum* by structured
750 rearrangement of *var* genes during mitosis. *PLoS Genet.* **10**, e1004812 (2014).
751 32. M. Zhang, C. Wang, T. D. Otto, J. Oberstaller, X. Liao, S. R. Adapa, K. Udenze, I. F.
752 Bronner, D. Casandra, M. Mayho, J. Brown, S. Li, J. Swanson, J. C. Rayner, R. H. Y.
753 Jiang, J. H. Adams, Uncovering the essential genes of the human malaria parasite
754 *Plasmodium falciparum* by saturation mutagenesis. *Science* **360**, (2018).
755 33. V. Thakur, M. Asad, S. Jain, M. E. Hossain, A. Gupta, I. Kaur, S. Rathore, S. Ali, N. J.
756 Khan, A. Mohmmed, Eps15 homology domain containing protein of *Plasmodium*
757 *falciparum* (PfEHD) associates with endocytosis and vesicular trafficking towards neutral
758 lipid storage site. *Biochim. Biophys. Acta* **1853**, 2856-2869 (2015).
759 34. R. C. Henrici, R. L. Edwards, M. Zoltner, D. A. van Schalkwyk, M. N. Hart, F. Mohring,
760 R. W. Moon, S. D. Nofal, A. Patel, C. Flueck, D. A. Baker, A. R. Odom John, M. C. Field,
761 C. J. Sutherland, The *Plasmodium falciparum* artemisinin susceptibility-associated AP-2
762 adaptin mu subunit is clathrin independent and essential for schizont maturation. *mBio* **11**,
763 e02918-02919 (2020).
764 35. T. Yang, S. Ottilie, E. S. Istvan, K. P. Godinez-Macias, A. K. Lukens, B. Baragana, B.
765 Campo, C. Walpole, J. C. Niles, K. Chibale, K. J. Dechering, M. Llinas, M. C. S. Lee, N.
766 Kato, S. Wyllie, C. W. McNamara, F. J. Gamo, J. Burrows, D. A. Fidock, D. E. Goldberg,
767 I. H. Gilbert, D. F. Wirth, E. A. Winzeler, C. Malaria Drug Accelerator, MalDA,
768 accelerating malaria drug discovery. *Trends Parasitol.* **Feb 26**, S1471-4922(1421)00012-
769 X (2021).
770 36. C. Snyder, J. Chollet, J. Santo-Tomas, C. Scheurer, S. Wittlin, In vitro and in vivo
771 interaction of synthetic peroxide RBx11160 (OZ277) with piperaquine in *Plasmodium*
772 models. *Exp. Parasitol.* **115**, 296-300 (2007).
773 37. E. H. Ekland, J. Schneider, D. A. Fidock, Identifying apicoplast-targeting antimalarials
774 using high-throughput compatible approaches. *FASEB J.* **25**, 3583-3593 (2011).

38. M. Vanaerschot, J. M. Murithi, C. F. A. Pasaje, S. Ghidelli-Disse, L. Dwomoh, M. Bird, N. Spottiswoode, N. Mittal, L. B. Arendse, E. S. Owen, K. J. Wicht, G. Siciliano, M. Bosche, T. Yeo, T. R. S. Kumar, S. Mok, E. F. Carpenter, M. J. Giddins, O. Sanz, S. Ottilie, P. Alano, K. Chibale, M. Llinas, A. C. Uhlemann, M. Delves, A. B. Tobin, C. Doerig, E. A. Winzeler, M. C. S. Lee, J. C. Niles, D. A. Fidock, Inhibition of resistance-refractory *P. falciparum* kinase PKG delivers prophylactic, blood stage, and transmission-blocking antiplasmodial activity. *Cell Chem. Biol.* **27**, 806-816 e808 (2020).

39. M. Karyana, L. Burdarm, S. Yeung, E. Kenangalem, N. Wariker, R. Maristela, K. G. Umana, R. Vemuri, M. J. Okoseray, P. M. Penttinen, P. Ebsworth, P. Sugiarto, N. M. Anstey, E. Tjitra, R. N. Price, Malaria morbidity in Papua Indonesia, an area with multidrug resistant *Plasmodium vivax* and *Plasmodium falciparum*. *Malar. J.* **7**, 148 (2008).

40. B. Russell, F. Chalfein, B. Prasetyorini, E. Kenangalem, K. Piera, R. Suwanarusk, A. Brockman, P. Prayoga, P. Sugiarto, Q. Cheng, E. Tjitra, N. M. Anstey, R. N. Price, Determinants of in vitro drug susceptibility testing of *Plasmodium vivax*. *Antimicrob. Agents Chemother.* **52**, 1040-1045 (2008).

41. J. Marfurt, F. Chalfein, P. Prayoga, F. Wabiser, E. Kenangalem, K. A. Piera, D. P. Fairlie, E. Tjitra, N. M. Anstey, K. T. Andrews, R. N. Price, Ex vivo activity of histone deacetylase inhibitors against multidrug-resistant clinical isolates of *Plasmodium falciparum* and *P. vivax*. *Antimicrob. Agents Chemother.* **55**, 961-966 (2011).

42. J. Marfurt, F. Chalfein, P. Prayoga, F. Wabiser, E. Kenangalem, K. A. Piera, B. Machunter, E. Tjitra, N. M. Anstey, R. N. Price, Ex vivo drug susceptibility of ferroquine against chloroquine-resistant isolates of *Plasmodium falciparum* and *P. vivax*. *Antimicrob Agents Chemother* **55**, 4461-4464 (2011).

43. M. Smilkstein, N. Sriwilaijaroen, J. X. Kelly, P. Wilairat, M. Riscoe, Simple and inexpensive fluorescence-based technique for high-throughput antimalarial drug screening. *Antimicrob. Agents Chemother.* **48**, 1803-1806 (2004).

44. M. Vanaerschot, L. Lucantoni, T. Li, J. M. Combrinck, A. Ruecker, T. R. S. Kumar, K. Rubiano, P. E. Ferreira, G. Siciliano, S. Gulati, P. P. Henrich, C. L. Ng, J. M. Murithi, V. C. Corey, S. Duffy, O. J. Lieberman, M. I. Veiga, R. E. Sinden, P. Alano, M. J. Delves, K. Lee Sim, E. A. Winzeler, T. J. Egan, S. L. Hoffman, V. M. Avery, D. A. Fidock,

Hexahydroquinolines are antimalarial candidates with potent blood-stage and transmission-blocking activity. *Nat. Microbiol.* **2**, 1403-1414 (2017).

45. S. H. Adjalley, G. L. Johnston, T. Li, R. T. Eastman, E. H. Ekland, A. G. Eappen, A. Richman, B. K. Sim, M. C. Lee, S. L. Hoffman, D. A. Fidock, Quantitative assessment of *Plasmodium falciparum* sexual development reveals potent transmission-blocking activity by methylene blue. *Proc. Natl. Acad. Sci. USA* **108**, E1214-1223 (2011).

46. E. Yoo, C. J. Schulze, B. H. Stokes, O. Onguka, T. Yeo, S. Mok, N. F. Gnadig, Y. Zhou, K. Kurita, I. T. Foe, S. M. Terrell, M. J. Boucher, P. Cieplak, K. Kumpornsin, M. C. S. Lee, R. G. Linington, J. Z. Long, A. C. Uhlemann, E. Weerapana, D. A. Fidock, M. Bogyo, The antimalarial natural product Salinipostin A identifies essential alpha/beta serine hydrolases involved in lipid metabolism in *P. falciparum* parasites. *Cell Chem. Biol.* **27**, 143-157 (2020).

47. D. A. Fidock, T. Nomura, T. E. Wellems, Cycloguanil and its parent compound proguanil demonstrate distinct activities against *Plasmodium falciparum* malaria parasites transformed with human dihydrofolate reductase. *Mol. Pharmacol.* **54**, 1140-1147 (1998).

48. S. H. Adjalley, M. C. Lee, D. A. Fidock, A method for rapid genetic integration into *Plasmodium falciparum* utilizing mycobacteriophage Bxb1 integrase. *Methods Mol. Biol.* **634**, 87-100 (2010).

49. D. A. Fidock, T. E. Wellems, Transformation with human dihydrofolate reductase renders malaria parasites insensitive to WR99210 but does not affect the intrinsic activity of proguanil. *Proc. Natl. Acad. Sci. USA* **94**, 10931-10936 (1997).

50. C. B. Mamoun, I. Y. Gluzman, S. Goyard, S. M. Beverley, D. E. Goldberg, A set of independent selectable markers for transfection of the human malaria parasite *Plasmodium falciparum*. *Proc. Natl. Acad. Sci. USA* **96**, 8716-8720 (1999).

51. P. Wang, Q. Wang, P. F. Sims, J. E. Hyde, Rapid positive selection of stable integrants following transfection of *Plasmodium falciparum*. *Mol. Biochem. Parasitol.* **123**, 1-10 (2002).

52. A. S. Nasamu, A. Falla, C. F. A. Pasaje, B. A. Wall, J. C. Wagner, S. M. Ganesan, S. J. Goldfless, J. C. Niles, An integrated platform for genome engineering and gene expression perturbation in *Plasmodium falciparum*. *Sci. Rep.* **11**, 342 (2021).

53. K. Deitsch, C. Driskill, T. Wellems, Transformation of malaria parasites by the spontaneous uptake and expression of DNA from human erythrocytes. *Nucleic Acids Res.* **29**, 850-853 (2001).

54. D. A. Fidock, T. Nomura, A. K. Talley, R. A. Cooper, S. M. Dzekunov, M. T. Ferdig, L. M. Ursos, A. B. Sidhu, B. Naude, K. W. Deitsch, X. Z. Su, J. C. Wootton, P. D. Roepe, T. E. Wellems, Mutations in the *P. falciparum* digestive vacuole transmembrane protein PfCRT and evidence for their role in chloroquine resistance. *Mol. Cell* **6**, 861-871 (2000).

55. A. F. Cowman, S. Karcz, D. Galatis, J. G. Culvenor, A P-glycoprotein homologue of *Plasmodium falciparum* is localized on the digestive vacuole. *J. Cell Biol.* **113**, 1033-1042 (1991).

56. G. Cremer, L. K. Basco, J. Le Bras, D. Camus, C. Slomianny, *Plasmodium falciparum*: detection of P-glycoprotein in chloroquine-susceptible and chloroquine-resistant clones and isolates. *Exp. Parasitol.* **81**, 1-8 (1995).

57. M. Klemba, W. Beatty, I. Gluzman, D. E. Goldberg, Trafficking of plasmepsin II to the food vacuole of the malaria parasite *Plasmodium falciparum*. *J. Cell Biol.* **164**, 47-56 (2004).

58. P. N. Tran, S. H. Brown, M. Rug, M. C. Ridgway, T. W. Mitchell, A. G. Maier, Changes in lipid composition during sexual development of the malaria parasite *Plasmodium falciparum*. *Malar. J.* **15**, 73 (2016).

59. N. M. Palacpac, Y. Hiramine, F. Mi-ichi, M. Torii, K. Kita, R. Hiramatsu, T. Horii, T. Mitamura, Developmental-stage-specific triacylglycerol biosynthesis, degradation and trafficking as lipid bodies in *Plasmodium falciparum*-infected erythrocytes. *J. Cell Sci.* **117**, 1469-1480 (2004).

60. K. S. Bane, S. Lepper, J. Kehrer, J. M. Sattler, M. Singer, M. Reinig, D. Klug, K. Heiss, J. Baum, A. K. Mueller, F. Frischknecht, The actin filament-binding protein coronin regulates motility in *Plasmodium* sporozoites. *PLoS Pathog.* **12**, e1005710 (2016).

61. J. R. Gallagher, S. T. Prigge, *Plasmodium falciparum* acyl carrier protein crystal structures in disulfide-linked and reduced states and their prevalence during blood stage growth. *Proteins* **78**, 575-588 (2010).

62. E. Mouray, M. Moutiez, S. Girault, C. Sergheraert, I. Florent, P. Grellier, Biochemical properties and cellular localization of *Plasmodium falciparum* protein disulfide isomerase. *Biochimie* **89**, 337-346 (2007).
63. A. Wandinger-Ness, M. Zerial, Rab proteins and the compartmentalization of the endosomal system. *Cold Spring Harb. Perspect. Biol.* **6**, a022616 (2014).
64. H. Stenmark, Rab GTPases as coordinators of vesicle traffic. *Nat. Rev. Mol. Cell Biol.* **10**, 513-525 (2009).
65. J. Kim, Y. Z. Tan, K. J. Wicht, S. K. Erramilli, S. K. Dhingra, J. Okombo, J. Vendome, L. M. Hagenah, S. I. Giacometti, A. L. Warren, K. Nosol, P. D. Roepe, C. S. Potter, B. Carragher, A. A. Kossiakoff, M. Quick, D. A. Fidock, F. Mancia, Structure and drug resistance of the *Plasmodium falciparum* transporter PfCRT. *Nature* **576**, 315-320 (2019).
66. C. Marin-Mogollon, A. M. Salman, K. M. J. Koolen, J. M. Bolscher, F. J. A. van Pul, S. Miyazaki, T. Imai, A. S. Othman, J. Ramesar, G. J. van Gemert, H. Kroeze, S. Chevalley-Maurel, B. Franke-Fayard, R. W. Sauerwein, A. V. S. Hill, K. J. Dechering, C. J. Janse, S. M. Khan, A *P. falciparum* NF54 reporter line expressing mCherry-luciferase in gametocytes, sporozoites, and liver-stages. *Front Cell Infect Microbiol* **9**, 96 (2019).
67. M. J. Delves, U. Straschil, A. Ruecker, C. Miguel-Blanco, S. Marques, A. C. Dufour, J. Baum, R. E. Sinden, Routine in vitro culture of *P. falciparum* gametocytes to evaluate novel transmission-blocking interventions. *Nat Protoc* **11**, 1668-1680 (2016).

Fig. 1

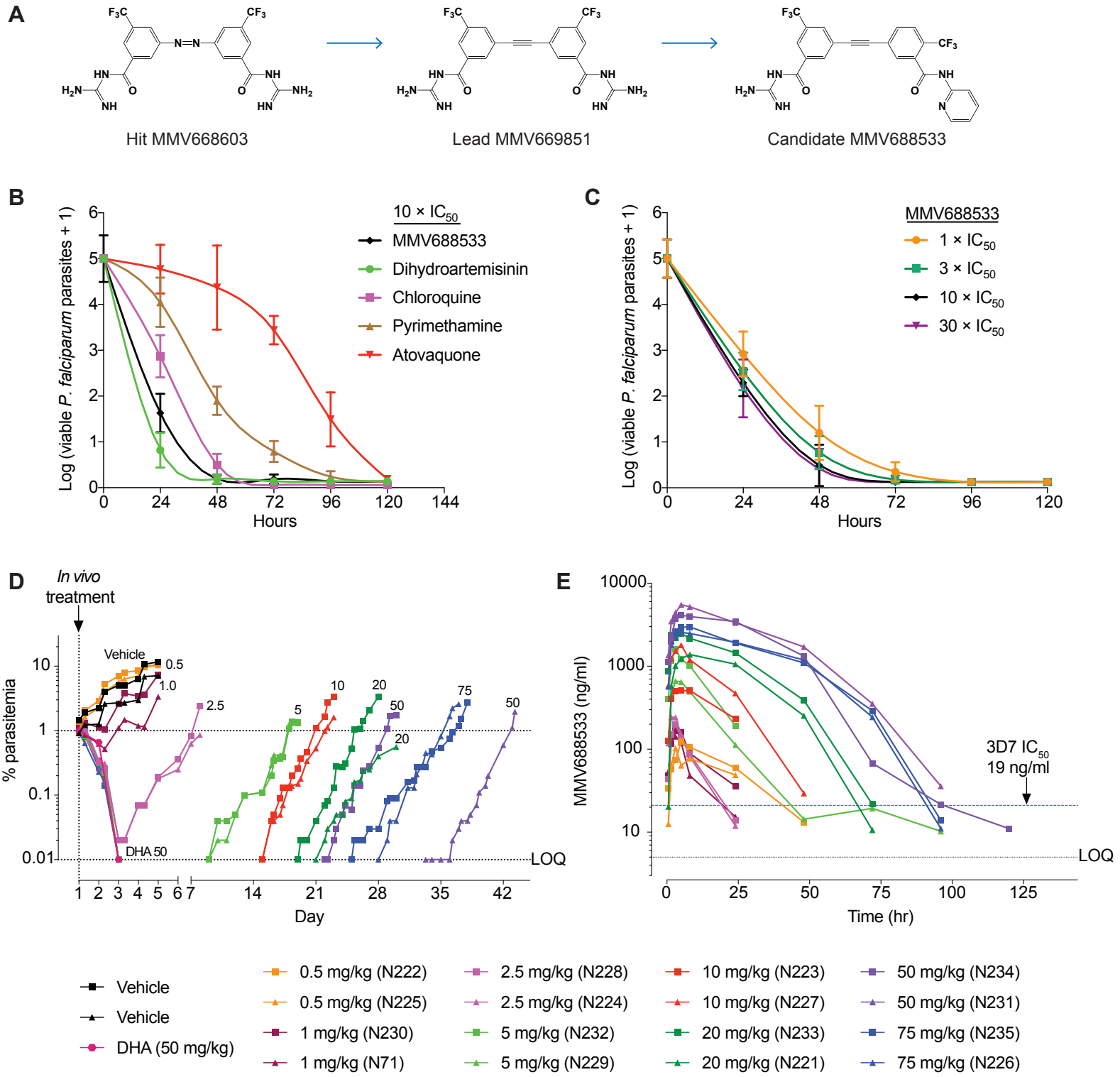
A
Hit MMV668603
Lead MMV669851
Candidate MMV688533
B
Log (viable P. falciparum parasites + 1)
Hours
10 × IC50
MMV688533
Dihydroartemisinin
Chloroquine
Pyrimethamine
Atovaquone
C
Log (viable P. falciparum parasites + 1)
Hours
MMV688533
1 × IC50
3 × IC50
10 × IC50
30 × IC50
D
In vivo treatment
% parasitemia
Day
Vehicle
DHA 50
LOQ
E
MMV688533 (ng/ml)
Time (hr)
3D7 IC50 19 ng/ml
LOQ
Vehicle
Vehicle
DHA (50 mg/kg)
0.5 mg/kg (N222)
0.5 mg/kg (N225)
1 mg/kg (N230)
1 mg/kg (N71)
2.5 mg/kg (N228)
2.5 mg/kg (N224)
5 mg/kg (N232)
5 mg/kg (N229)
10 mg/kg (N223)
10 mg/kg (N227)
20 mg/kg (N233)
20 mg/kg (N221)
50 mg/kg (N234)
50 mg/kg (N231)
75 mg/kg (N235)
75 mg/kg (N226)

Fig. 2

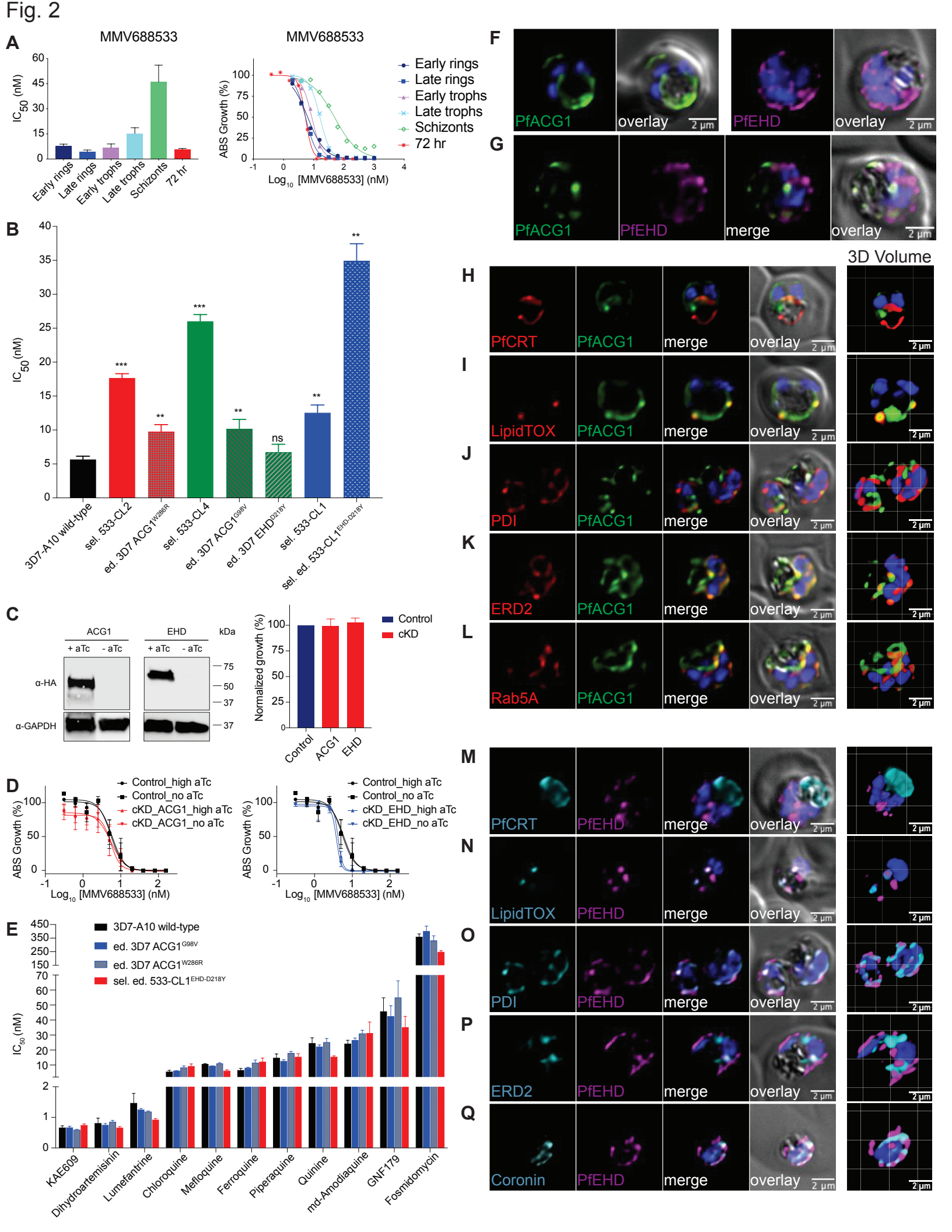
A
MMV688533
MMV688533
IC50 (nM)
Early rings
Late rings
Early trophs
Late trophs
Schizonts
72 hr
ABS Growth (%)
Log10 [MMV688533] (nM)
B
IC50 (nM)
3D7-A10 wild-type
sel. 533-CL2
ed. 3D7 ACG1W286R
sel. 533-CL4
ed. 3D7 ACG1G98V
ed. 3D7 EHDD218Y
sel. 533-CL1
sel. ed. 533-CL1EHD-D218Y
C
ACG1
EHD
kDa
+ aTc
- aTc
α-HA
α-GAPDH
Normalized growth (%)
Control
cKD
D
Control_high aTc
Control_no aTc
cKD_ACG1_high aTc
cKD_ACG1_no aTc
cKD_EHD_high aTc
cKD_EHD_no aTc
ABS Growth (%)
Log10 [MMV688533] (nM)
E
3D7-A10 wild-type
ed. 3D7 ACG1G98V
ed. 3D7 ACG1W286R
sel. ed. 533-CL1EHD-D218Y
IC50 (nM)
KAE609
Dihydroartemisinin
Lumefantrine
Chloroquine
Mefloquine
Ferroquine
Piperaquine
Quinine
md-Amodiaquine
GNF179
Fosmidomycin
F
PfACG1
overlay
PfEHD
G
merge
H
PfCRT
I
LipidTOX
J
PDI
K
ERD2
L
Rab5A
M
N
O
P
Q
Coronin
3D Volume
2 μm

Supplementary Materials

The antimalarial MMV688533 provides single-dose cures with a high barrier to *Plasmodium falciparum* parasite resistance

James M. Murithi[§], Cécile Pascal[§], Jade Bath, Xavier Boulenc, Nina F. Gnädig, Charisse F.A. Pasaje, Kelly Rubiano, Tomas Yeo, Sachel Mok, Sylvie Klieber, Paul Desert, Maria Belen Jimenez-Diaz, Jutta Marfurt, Mélanie Rouillier, Mohammed Cherkaoui, Nathalie Gobeau, Sergio Wittlin, Anne-Catrin Uhlemann, Ric N. Price, Grennady Wirjanata, Rintis Noviyanti, Patrick Tumwebaze, Roland A. Cooper, Philip J. Rosenthal, Laura M. Sanz, Francisco Javier Gamo, Jayan Joseph, Shivendra Singh, Sridevi Bashyam, Jean Michel Augereau, Elie Giraud, Tanguy Bozec, Thierry Vermat, Gilles Tuffal, Jean-Michel Guillon, Jérôme Menegotto, Laurent Sallé, Guillaume Louit, Marie-José Cabanis, Marie Françoise Nicolas, Michel Doubovetzky, Rita Merino, Nadir Bessila, Iñigo Angulo-Barturen, Delphine Baud, Lidiya Bebrevska, Fanny Escudié, Jacquin C. Niles, Benjamin Blasco, Simon Campbell, Gilles Courtemanche, Laurent Fraisse, Alain Pellet, David A. Fidock*, Didier Leroy*

[§]Co-first authors. *Co-corresponding authors, DAF: df2260@cumc.columbia.edu; DL: leroyd@mmv.org

This file includes:

Materials and Methods

Synthesis of MMV688533

Step 1. $Pd(PPh_3)_2Cl_2$ (4.96 g, 7.07 mmol) and cuprous iodide (1.34 g, 7.06 mmol) were added to a degassed solution of methyl 3-bromo-5-(trifluoromethyl)benzoate (20.0 g, 70.67 mmol) and trimethylsilylacetylene (17.4 g, 176.67 mmol) in 100 mL of acetonitrile in a sealed tube. The tube was degassed again and heated at 70 °C for 2 h. The reaction mixture was cooled and filtered through a celite bed. The filtrate was concentrated in vacuum and the residue purified through silica gel (60-120 mesh) column chromatography using petroleum ether to generate a 3-Trifluoromethyl-5-trimethylsilanylethynyl-benzoic acid methyl ester (14 g, yield 66 %) as yellow liquid.

Step 2. Potassium carbonate (0.58 g 4.2 mmol) was added to a solution of 3-Trifluoromethyl-5-trimethylsilanylethynyl-benzoic acid 2-methyl ester (14.0 g, 46.60 mmol) in 50 mL methanol and stirred at room temperature for 20 minutes. The reaction mixture was concentrated under reduced pressure. The residue was diluted with 100 mL ethyl acetate, washed with water and brine and dried over anhydrous sodium sulphate and concentrated to yield 3-Ethynyl-5-trifluoromethyl-benzoic acid methyl ester (11 g, yield 61%) as a brown liquid.

Step 3. Lithium hydroxide (6.0 g, 144.10 mmol) was added to an ice cooled solution of 3-Ethynyl-5-trifluoromethyl-benzoic acid methyl ester (11.0 g, 48.03 mmol) in 50 mL tetrahydrofuran and 25 mL water and stirred at room temperature for 3 h. The reaction mixture was concentrated and acidified with aqueous citric acid solution. The precipitated solid was filtered, washed with water and dried to generate 3-Ethynyl-5-trifluoromethyl-benzoic acid (9.2 g, yield 78%) as pale brown solid.

Step 4. Dicyclohexylcarbodiimide (13.28 g, 64.48 mmol) and pentafluorophenol (11.8 g, 64.48 mmol) in 50 mL tetrahydrofuran was added to a solution of 3-Ethynyl-5-trifluoromethyl-benzoic acid (9.2 g, 42.99 mmol) and stirred at room temperature for 3 h. Upon the completion of the reaction, the

mixture was cooled in an ice bath and the precipitated dicyclohexylurea removed by filtration. The filtrate was concentrated and purified using a silica gel (60-120 mesh) column chromatography using ethyl acetate in petroleum ether, producing 3-Ethynyl-5-trifluoromethyl-benzoic acid pentafluorophenyl ester (13.6 g, yield 83%) as an off-white solid.

Step 5. Monobocguanidine (6.82 g, 42.94 mmol) was added to a solution of 3-Ethynyl-5-trifluoromethyl-benzoic acid pentafluorophenyl ester (13.6 g, 35.78 mmol) in 50 mL tetrahydrofuran and stirred at room temperature for 4 h. After the completion of the reaction, the mixture was evaporated and purified through silica gel (60-120 mesh) column chromatography using ethyl acetate in petroleum ether to generate tert-butylN-[N-[3-ethynyl-5-(trifluoromethyl)benzoyl] carbami-midoyl]carbamate (8.2 g, yield 64 %) as an off white solid.

Step 6: 10 mL of concentrated H_2SO_4 was added dropwise to a solution of 5-bromo-2-iodobenzoic acid (100 g, 305.89 mmol) in 800 mL MeOH. The mixture was refluxed for 16 h and then concentrated. The residue was dissolved in 1 L ethyl acetate. The organic layer was washed with saturated $NaHCO_3$ and 3 × 200 mL brine, dried over Na_2SO_4, filtered and concentrated to generate 5-Bromo-2-iodo-benzoic acid methyl ester (101.4 g, yield 90%) as yellow solid.

Step 7. Copper (I) bromide (1.21g, 8.45 mmol) was added to a solution of 5-Bromo-2-iodo-benzoic acid methyl ester (24 g, 70.4 mmol) and methyl 2,2-difluoro-2-(fluorosulfonyl)acetate (13.5 mL, 105.6 mmol) in 80 mL N-methyl-2-pyrrolidinone. The reaction mixture was stirred at 100 °C for 5 h. The reaction was filtered and partitioned between ethyl acetate and brine. The aqueous layer was extracted with ethyl acetate, and the organic layers were combined and dried over Na_2SO_4. After filtration, the solvent was removed *in vacuo*. The residue was purified by silica gel column (0-4% Ethyl acetate in Petroleum ether) to give the 5-Bromo-2-trifluoromethyl-benzoic acid methyl ester (119.2 g, yield 96%) as yellow oil.

Step 8. Lithium hydroxide (4.4 g, 104.76 mmol) was added to an ice cooled solution of 5-Bromo-2-trifluoromethyl-benzoic acid methyl ester (9.1 g, 35.68 mmol) in 20 mL tetrahydrofuran and 10 mL water and stirred at room temperature for 3 h. The reaction mixture was concentrated and acidified with aqueous citric acid solution. The precipitated solid was filtered, washed with water and dried to produce 5-Bromo-2-trifluoromethyl-benzoic acid (8 g, yield 95%) as pale yellow solid.

Step 9. 5-Bromo-2-trifluoromethyl-benzoic acid (8.0 g, 29.74 mmol) in 40 mL thionyl chloride solution was heated to reflux for 3 h. The completion of reaction (conversion of acid chloride to methyl ester) was observed by thin layer chromatography (TLC). Thionyl chloride was evaporated and the residue added to the reaction mixture containing 2-amino pyridine (3.2 g, 32.71 mmol), triethyl amine (12.44 mL, 89.21 mmol) in dry 80 mL ethyl acetate at 0 ºC. The reaction mixture was stirred at room temperature for 12h. Reaction completion was observed by TLC. The reaction mixture was then added to 200 mL water and extracted with 2 × 200 mL ethyl acetate. The combined organic layer was washed with 2 × 100 mL water, brine, dried over sodium sulphate and evaporated. The crude material was purified by column chromatography using ethyl acetate in petroleum ether to generate 5-Bromo-N-pyridin-2-yl-2-trifluoromethyl-benzamide (5.1 g, yield 49%) as off white solid.

Step 10. 5-Bromo-N-pyridin-2-yl-2-trifluoromethyl-benzamide intermediate (0.690 kg, 2 mol.), CuI (0.019 kg, 0.1 mol.), $Pd(PPh_3)2Cl_2$ (0.140 kg, 0.2 mol.) and acetonitrile were mixed in a 6 L reactor under nitrogen. Tert-butyl N-[N-[3-ethynyl-5-(trifluoromethyl)benzoyl]carbamimidoyl]carbamate intermediate (0.924 kg, 2.6 mol) was added in 5 min on the suspension while stirring at 25 °C. The mixture was degassed under nitrogen bubbling for an additional 30 min while still stirring. Triethylamine (0.605 kg, 5.98 mol) was added in 17 min at 25 °C. An exotherm of + 6 °C was observed. The dropping funnel was washed with 0.5 L acetonitrile. The reaction mixture was heated at 45 °C and maintained for 2 h until tert-butyl N-[N-[3-ethynyl-5-(trifluoromethyl)benzoyl]-

carbamimidoyl]carbamate was < 1%. The suspension was then cooled to 10 °C at the rate of – 20 °C/h and maintained for 1 h. The expected intermediate tert-butyl N-[N-[3-[2-[3-(2-pyridyl-carbamoyl)-4-(trifluoromethyl)phenyl]ethynyl]-5-(trifluoromethyl)benzoyl]-carba-mimidoyl] carbamate was filtered and the cake was washed with 1.4 L acetonitrile followed by 0.7 L water. After drying by nitrogen flux overnight at 0.3 bar, tert-butyl N-[N-[3-[2-[3-(2-pyridylcarbamoyl)-4-(trifluoromethyl)phenyl]ethynyl]-5-(trifluoromethyl)benzoyl]carbamimidoyl]-carbamate was isolated (0.745 kg, yield 60%).

Step 11. A suspension of tert-butyl N-[N-[3-[2-[3-(2-pyridylcarbamoyl)-4-(trifluoromethyl) phenyl]-ethynyl]-5-trifluoromethyl)benzoyl]carbamimidoyl]carbamate (1.5 kg, 2.42 mol) in 14.5 L ethyl acetate was heated at 70 °C while stirring. Trifluoroacetic acid (2.2 kg, 19.30 mol) was added in 30 min at 70 °C. The dropping funnel was washed with 0.75 L ethyl. The reaction mixture was maintained for 22 h at 70 °C until tert-butyl N-[N-[3-[2-[3-(2-pyridylcarbamoyl)-4-(trifluoromethyl)-phenyl]ethynyl]-5-(trifluoromethyl)benzoyl]carbamimidoyl]carbamate was < 1%. After cooling at 20 °C the mixture was basified by addition of a solution of 28% NH_4OH in 1 h until pH was between 9-10. After an additional 15 min stirring, 11.3 L water were added and the phases separated. The organic layer was diluted with 45 L, 30 vol ethyl acetate and washed successively with an aqueous solution of sodium metabisulfite ($Na_2S_2O_5$ 0.15 kg in 15 L water) and 15 L water. An additional treatment with charcoal (Darco S51) was done. 56.37 kg of ethyl acetate solution was used for the next salification step.

Step 12. A part of the previous acetate solution of 5-((3-(carbamimidoylcarbamoyl)-5-(trifluoro-methyl)phenyl)ethynyl)-N-(pyridin-2-yl)-2-(trifluoromethyl)benzamide (0.958 kg, 1.844 mol,), which was estimated to be pure, was concentrated under a reduced pressure of 100 mbars and at 50 °C into 10 vol of ethyl acetate. An additional azeotropic drying was realized with 15 vol ethyl acetate.

The obtained 10 vol solution was heated at 50 °C, and then a seeding with 2% of 5-((3-(carbamimidoylcarbamoyl)-5-(trifluoromethyl)phenyl)ethynyl)-N-(pyridin-2-yl)-2-(trifluorom-ethyl)-benzamide malonic acid was done. A solution of malonic acid (0.192 kg, 1.144 mol.) in 2.8 L ethyl acetate was added in 30 min at 50 °C. The dropping funnel was washed with 0.4 L ethyl acetate and crystallization was observed during the addition of the acid. Stirring was maintained for 1 h at 50 °C and cooled to 10 °C at the rate of -20 °C/h. 5-((3-(carbamimidoylcarbamoyl)-5-(trifluoromethyl) phenyl)ethynyl)-N-(pyridin-2-yl)-2-(trifluoromethyl) benzamide malonic acid was isolated by a fast filtration and the cake was washed twice with 1 L ethyl acetate. The product was dried under nitrogen flux overnight to generate 5-((3-(carbamimidoylcarbamoyl)-5-(trifluoromethyl) phenyl)ethynyl)-N-(pyridin-2-yl)-2-(trifluoromethyl)benzamide malonic acid compound (1.096 kg, yield of 95.3%).

Nuclear magnetic resonance (NMR) and mass spectrometry (MS) analysis

^{1}H NMR and ^{13}C NMR data were recorded on a Bruker 400MHz AVANCE series or Bruker300 MHz DPX Spectrometer with $CDCl_3$ or DMSO-d6 or CD3OD as solvent. ^{1}H chemical shifts were referenced at 7.26 ppm for $CDCl_3$, 2.5 ppm for DMSO-d6 and 3.3 ppm for CD3OD. ^{13}C chemical shifts were referenced at 77 ppm for $CDCl_3$, 39 ppm for DMSO-d6 and 44 ppm for CD3OD, and obtained with ^{1}H decoupling. Multiplicities are abbreviated as follows: singlet (s), doublet (d), triplet (t), quartet (q), doublet-doublet (dd), quintet (quint), sextet (sextet), septet (septet), multiplet (m), and broad (br).

MS data were measured on Agilent 1200/1260 Series LC/MSD mass spectrometer with the following settings. Column: Zorbax XDB C18 (50 X 4.6) mm, 5µm or Acquity BEH C18 (50 x 2,1 mm; 1.7 µm). Mobile phase: Solvent A: 0.1% Formic Acid in Milli-Q water (or) 0.1% Trifluoroacetic acid in

Milli-Q-water. Solvent B: Acetonitrile. Flow rate: 1.5 mL/min. Injection Volume: 2 µL. Wavelength: Maximum chromatogram (210-400nm). Run time: 6.0 min. Ionization source: Multi-mode (ESI and APCI). Purity was measured on an Agilent 1200/1260 Series HPLC spectrometer. Column: C18 (250 X 4.6) mm, 5µm (or) C18 (150 X 4.6) mm, 5µm. Mobile phase: Solvent A: 10 mM ammonium acetate in Milli-Q water (or) 0.1% Trifluoroacetic acid in Milli-Q-water; Solvent B: Acetonitrile. Flow rate: 1.0mL/min. Injection Volume: 2 µL. Wavelength: Maximum chromatogram (210-400 nm). Run time: 30 min.

For compound 1c, MS data were measured with UPLC-SQD (Simple Quad, from Waters). Column: Acquity BEH C18 (50 x 2,1 mm; 1.7 µm). Mobile phase: Solvent A: H_2O+0.05% TFA; Solvent B: CH_3CN+0.035% TFA. Flow rate; 1 mL/min. UV Detection: l = 220 nm. MS detection (Simple Quad) ionization: ESI + Electrospray First / Last Mass (uma) FS: 160 / 1200 uma. Capillary voltage (KV): 3.5.Cone. (V): 20. Source Temperature: 150°C. Desolvation temperature: 500°C. Desolvation gas flow (L/hr): 1200. Cone gas flow (L/hr): 100. LM 1 resolution: 13.00. HM1 resolution: 13.00. Ion energy1: 0.20.

For the intermediate 5-Bromo-2-iodo-benzoic acid methyl ester (step 6), LC-MS was measured as follows: Column: XBridge C18,4.6*50mm, 3.5 µm Mobile phase: 10 mM NH_4HCO_3 (A) / acetonitrile (B). Elution program: Gradient from 5 to 95% of B in 1.6 min at 1.8 mL/min. Temperature: 50ºC. Detection: UV (214, 4 nm). MS: ESI, Positve mode, 110 to 1000 amu.

Determination of ex vivo potency against *P. falciparum* and *P. vivax*

Compounds. MMV688533 (Sanofi, Toulouse, France) and the reference antimalarial drugs chloroquine, piperaquine, mefloquine, and artesunate (provided by the WWARN QA/QC Reference

Material Programme), were prepared as 1 mg/mL stock solutions in dimethyl sulfoxide (DMSO) or H_2O according to the manufacturers' instructions. Drug plates were pre-dosed by diluting the compounds in 50% methanol followed by lyophilization and storage at 4 °C.

Field location and sample collection. In Papua Indonesia, *Plasmodium* isolates were collected from patients attending malaria clinics in Timika, a region endemic for multidrug-resistant strains of *P. vivax* and *P. falciparum* (*39, 40*). Patients with symptomatic malaria were recruited into the study if singly infected with *P. falciparum* or *P. vivax*, with a parasitemia of between 2,000 and 80,000 parasites per μL, and a majority (>60%) of parasites present as rings. Venous blood (5 mL) was collected by venipuncture and host white blood cells were removed with Plasmodipur filters (EuroProxima B.V., The Netherlands). Packed infected RBCs were then used for ex vivo drug susceptibility assays. In Uganda, *Plasmodium* isolates were collected from patients aged 6 months or older presenting to the Tororo District Hospital, Tororo District, or Masafu Hospital in the Busia District, with a clinical syndrome suggestive of malaria and *Plasmodium falciparum* parasites identified in blood by microscopy. Informed consent was obtained from patients and/or primary care givers (depending on age).

Ex vivo drug susceptibility assays. In Papua Indonesia, drug susceptibility was measured in *P. vivax* and *P. falciparum* isolates using a protocol modified from the WHO microtest (*40-42*). In brief, 200 μL of a 2% hematocrit of blood media mixture, consisting of RPMI 1640 medium plus 10% AB^+ human serum for *P. falciparum* or McCoy's 5A medium plus 20% AB^+ human serum for *P. vivax* was added to each well of pre-dosed drug plates containing 11 serial concentrations (2-fold dilutions) of the test antimalarials (maximum concentration shown in brackets) chloroquine (2,993 nM),

piperaquine (1,029 nM), mefloquine (338 nM), artesunate (49 nM), and MMV688533 (237 nM). A candle jar was used to mature the parasites at 37 °C for 35-56 h. Incubations were stopped when >40% of the ring-stage parasites had reached the mature schizont stage in the drug-free control wells, as determined by light microscopy. Parasite growth was quantified by nucleic acid staining and parasitemias were measured using flow cytometry. Parasite growth was quantified for each drug concentration and normalized to the control well. The dose-response data were analyzed using nonlinear regression analysis and the half-maximal inhibition of growth (IC_{50}) values derived using an inhibitory sigmoid E_{max} model (In vitro Analysis and Reporting Tool; IVART7). Ex vivo IC_{50} data were only used from predicted curves where the E_{max} and E_0 were within 15% of 100 and 1, respectively. The drug plate quality was assured by running schizont maturation assays with the *P. falciparum* chloroquine-resistant strain K1 and the chloroquine-sensitive strain FC27. For data quality control, raw flow cytometry values were analyzed by two independent operators and compared. If the raw dose-response data derived by the two operators led to a dramatic shift in IC_{50} estimates for any of the drugs, they were reviewed and adjusted by a third operator. Ethical approval for this study was obtained from the Eijkman Institute Research Ethics Commission of the Eijkman Institute for Molecular Biology, Jakarta, Indonesia; the Human Research Ethics Committee of the Northern Territory Department of Health & Families; and the Menzies School of Health Research, Darwin, Australia.

In Africa, drug susceptibility was measured in *P. vivax* and *P. falciparum* isolates using a protocol summarized as follows: All MMV compounds were dissolved in DMSO to a final concentration of 0.5-10 mM and stored at -20°C. On the day of assay, 2 µL of DMSO stocks drug were diluted in 498 µL complete RPMI media (RPMI 1640 medium supplemented with 25 mM HEPES, 0.2%

NaHCO3, 0.1 mM hypoxanthine, 100 µg/mL gentamicin, and 0.5% Albumax I [Invitrogen]). Diluted drugs were not stored for longer than 24 h. Drugs were serially diluted 3-fold in 96-well assay plates in complete media containing 0.4% DMSO, to a final volume of 50 µL, in columns 1-10. Column 11 contained drug-free controls while column 12 contained uninfected RBC controls. Parasitized whole blood samples were washed 3 times with RPMI (w/o Albumax) media at 37 °C and then resuspended in fresh RPMI media to a final hematocrit of 2%. 150 µL of the parasite culture was added to each well into the assay plate for final parameters of 0.2% parasitemia and 2% hematocrit. Plates were incubated for 72 h in a humidified modular incubator under a tri-gas mixture (5% O_2, 5% CO_2, 90% N_2) at 37 °C. Plates were then stained with SYBR Green I and fluorescence determined using a BMG Fluostar Optima plate reader at excitation 485 nm / emission 530 nm (*43*). Fluorescence data were curve fitted to estimate IC_{50} values (GraphPad Prism 7). For each isolate, a Z' factor was calculated from drug-free positive and negative controls (8 parasitized RBC wells and 8 uninfected RBC wells, respectively).

Determination of efficacy and pharmacokinetic profiles in the Pf SCID mouse model

Immunodeficient female NSG or NOG mice were engrafted with a minimum of 40% human erythrocytes circulating in peripheral blood during the entire experiment. Each mouse was inoculated with a 50%-75% hematocrit erythrocyte suspension (Basque Center of Transfusion and Human Tissues, Galdakao, Spain and Bank of Blood and Tissues, Barcelona, Spain) in RPMI1640 medium, 25% (vol/vol) decomplemented human serum, 3.1 mM hypoxanthine. Intraperitoneal (i.p.) and/or intravenous (i.v., via tail lateral vein) injections were done once daily until the end of the drug administration period. Humanized NSG or NOG mice were infected with peripheral blood from CO_2-euthanized donor mice harboring 5-10% parasitemia. The humanized mice of the efficacy study were

infected by inoculation of 0.3 mL of the infected-erythrocyte suspension by the lateral vein of the tail. For treatment, drug was administered at Day 1 (~1% patent parasitemia) (P0) by oral gavage (volume p.o. is 10 mL/kg body weight). To measure the therapeutic response, 2 µL peripheral tail blood from *P. falciparum*-infected mice were stained with TER-119-Phycoerythrine (marker of murine erythrocytes) and SYTO-16 (nucleic acid dye) and analyzed by flow cytometry (Attune NxT Acoustic Focusing Flow Cytometer, Invitrogen). Drug effect on circulating *P. falciparum* Pf3D70087/N9 parasites was assessed by microscopy (Giemsa-stained blood smears; 2 µL blood samples taken at 48 h and 96 h).

To assess the drug concentrations in mice, 25 µL samples of peripheral blood were taken at different times (usually 0.5, 1, 2, 4, 6 or 8 h and 23 h after the first dosing), mixed with 25 µL of MilliQ H_2O and immediately frozen on a thermal block at -80º C. The treated mice that reached the limit of detection by standard flow cytometry (<0.01% from total circulating erythrocytes) were maintained until day 60 of the assay with a chimerism >50% of total circulating erythrocytes by regular injection of human erythrocytes every 3 or 4 days. During the follow up period, 2 µL blood samples were taken every 2 or 3 days and analyzed by flow cytometry with a limit of quantification of 0.1%. The first day of parasitemia detection was recorded. The mice were deemed cured (free of detectable parasite) if no recrudescence was detected by day 60.

As biological controls; a) parasite growth in untreated and/or vehicle-treated individuals was evaluated from day 1 to 5; b) the parasite burden was measured from day 1 to 5 of the assay in individuals treated with a fixed dose of a standard antimalarial; and c) the distribution of parasitemia

at day 1 of the assay for all individual mice tested in the assay was compared to parasitemia distributions in previous experiments.

For data analysis, ED_{90} and AUC_{ED90} were defined and calculated according to (*14*). ED_{90} is the effective dose in mg/kg that reduced parasitemia by 90% at day 5 compared to vehicle-treated mice. AUC_{ED90} is the average estimated daily exposure that reduced parasitemia from peripheral blood at day 5 of the assay by 90% compared to vehicle-treated mice. The ED_{90} was calculated by fitting the variable Y= $\log_{10}$ [parasitemia at day 5 of the assay] and the variable X= $\log_{10}$ [dose level in mg/kg] defined as an ordered pair for every individual of the study. The AUC_{ED90} was calculated by fitting the variable Y= $\log_{10}$ [parasitemia at day 5 of the assay] and the variable X= $\log_{10}$ [AUC of compound during the first 23 h after the first drug administration, in ng·h/mL] defined as an ordered pair for every individual of the study. The equation used to fit the data is Y=Bottom + (Top-Bottom)/(1+10((LogED_{50}-X)×Hill Slope)). The ED_{90} and AUC_{ED90} were calculated by interpolation of the X value that corresponded to antilog10 [Y= "Top"-1] in each respective best fitted curve (*14*).

The time in days (te) and the average concentration in blood (C, in ng/mL) for killing all *P. falciparum* parasites in mice were interpolated from a multivariate logistic regression. The fitted function links the dichotomic response variable Therapeutic response (Tr), which takes Tri=0 if an individual shows recrudescence and Tri=1 if no recrudescence was detected at day 60 of the assay, and the explanatory variables te and C. These parameters offered direct empirical estimates of the time of exposure and concentration in blood to at least kill a defined number of circulating parasites, which was typically 10^8 per mouse. The regression formular is as follows: $(Tr=1|te,C)= 11+ e-(\alpha+\beta 1te+\beta 2C)$.

Data analysis was performed using GraphPad Prism 7.0 (GraphPad Software), Excel 2016 (Microsoft) and R free software (https://www.r-project.org). Phoenix WinNonlin vers.7.0 (Certara) was used for PK Non-Compartmental Analysis. Animal experiments performed at TAD were approved by The Art of Discovery Institutional Animal Care and Use Committee (TAD-IACUC). The Committee is certified by the Biscay County Government (Bizkaiko Foru Aldundia, Basque Country, Spain) to evaluate animal research projects from Spanish institutions according to point 43.3 from Royal Decree 53/2013, from the 1st of February (BOE-A-2013-1337). All experiments were carried out in accordance with European Directive 2010/63/EU. The results from the animal experiments are reported following ARRIVE guidelines. (https://www.nc3rs.org.uk/arrive-guidelines) except for disclosure of business trade confidential information.

Prediction of the efficacious dose in humans based on Pf SCID mouse PK/PD

The prediction of the first efficacious dose in human was based on: 1) minimum parasiticidal concentration (MPC) as evaluated from a population-based PK/PD modeling of experimental data from SCID mouse studies. At team at MMV used a NonMem software and another at Sanofi used a Monolix software to build a PK/PD model. Both teams reached a similar median estimate value of 20 ng/mL as the MPC; 2) K_{kill} of the compound as deduced from in vitro logPRR (5 in 48 h). However, a conservative approach was recommended by MMV to use a capped value of 3 based on values observed for endoperoxides when tested in human; 3) predicted human PK parameters as determined by an allometric approach. For the allometric scaling of clearance from animal data, two methods, Mahmood rules and Fixed exponent method, were used. These led to the prediction of a low to a very low MMV688533 clearance in humans 3.6 and 1.4 L/h respectively, that

corresponded to a total clearance of < 5% of hepatic blood flow. This in turn corresponded to a predicted half-life of 103 h and 277 h respectively in humans. The volume of distribution (Vdss) relying on allometry method with an exponent of 1, was predicted to be as large as 540 L for 70 kg human; 4) biopharmaceutical model (GastroPlus) used to estimate Fa% vs dose in human and verified on Rat & Dog PK data.

P. falciparum lines used for selections, drug assays and transfections

Asexual blood-stage parasites were cultured at 3% hematocrit in O^+ human erythrocytes in RPMI-1640 medium supplemented with 50 μM hypoxanthine, 2.25 g/L $NaHCO_3$, 2 mM L-glutamine, 25 mM HEPES, 0.5% (w/v) AlbuMAXII (Invitrogen) and 10 μg/mL gentamycin at 37 °C in flasks gassed with 5% O_2/5% CO_2/90% N_2. The *P. falciparum* 3D7-A10 and Dd2-B2 clones used for the selections and drug assays, and the NF54attB line used to express *pfacg1*-eGFP and *pfehd*-3×HA, have been previously reported (*15, 44, 45*).

Genome editing

Mutations in PfACG1 and PfEHD that were identified from the in vitro selections were validated by engineering them into the parental 3D7-A10 line using an "all-in-one" pDC2-based CRISPR/Cas9 plasmid ((*46*); **Fig. S2A**). The Cas9 in this plasmid is derived from *Streptococcus pyogenes,* has been codon optimized for *P. falciparum,* and is under the expression of a calmodulin promoter. The plasmid also contains a human *dhfr* (h*dhfr*) selectable marker (that confers resistance to WR99210) under a PcDT promoter, and the sequence encoding the guide RNA (gRNA) under a U6 promoter. Guide RNAs were selected using the online tool ChopChop based on their proximity to the mutation of interest, GC content, and absence of poly A/T tracks

(http://chopchop.cbu.uib.no). The gRNA primers were annealed with BbsI overhangs using PCR and cloned into a BbsI-linearized pDC2 CRISPR/Cas9 vector. The donor templates, also supplied on the same plasmid, had >300bp of homology flanking the mutation of interest. These fragments were first amplified by PCR and cloned into pGEM-T vectors to introduce shield mutations by site-directed mutagenesis. Shielded donor fragments were then amplified by PCR and cloned into the EcoRI/AatII-linearized pDC2 CRISPR/Cas9 vector by In-Fusion cloning (Takara). Finally, the plasmids were midi-prepped for transfections.

Parasites were electroporated with purified circular plasmid DNA as described (*47*). Briefly, a 2.5 mL culture of 3D7-A10 or sel. 533-CL1 (≥ 5% rings) was washed and resuspended in 220 µL 1× Cytomix. This mixture was then added to 50 µg of plasmid DNA and electroporated at a voltage of 0.31 kV and capacitance of 950 µF inside 2 mm gap cuvettes (Bio-Rad) using a Gene-Pulser (Bio-Rad) (*48*). Starting one day after the transfections, the cultures were selected for six days with 2.5 nM WR99210 (*49*) and maintained thereafter in complete media until recrudescence. Gene editing was assessed via Sanger sequencing of blood PCR (Bioline) from bulk cultures. Edited parasite clones were obtained by limiting dilution. The parasites were then assayed for resistance to MMV688533 using flow cytometry.

Both the mycobacteriophage Bxb1 serine integrase system (*48*) and CRISPR/Cas9 gene editing tools were used to generate the doubly-tagged parasite line expressing PfACG1-eGFP and PfEHD-3×HA fusion proteins. Briefly, NF54attB parasites (*45*) were first co-transfected with an integrase-expressing plasmid pINT and a donor attP-containing plasmid pDC2-*pfacg1*-eGFP. This donor plasmid also contained a blasticidin S-deaminase (BSD) selectable marker that confers resistance

to blasticidin hydrochloride (*50*). The integrase plasmid pINT contained a Neomycin selectable marker that confers resistance to geneticin (G418; (*51*); **Fig. S2B**). Transfections were done as described above and the cultures maintained in 250 μg/mL G418 + 2 μg/mL BSD media for six days post-transfection, followed by 2μg/mL BSD media until recrudescence. Sorbitol-synchronized eGFP-tagged ring-stage clonal parasites obtained by limiting dilution were then transfected with the codon-optimized all-in-one plasmid containing a 1.1kb *pfehd* donor fragment consisting of two 3' homology sequences flanking the 3×HA tag (**Fig. S2C**). These transfections were selected with 2.5 nM WR99210 until recrudescence. Successful gene tagging was confirmed via PCR, Sanger sequencing and immunofluorescence assays.

Conditional knock-down (cKD) parasite studies

Generation of cKD parasite lines. To investigate the interaction between MMV688533 and PfACG1 and PfEHD genes, we utilized CRISPR/Cas9 to generate parasite cell lines stably expressing the TetR-DOZI-RNA aptamer module for conditional regulation of target gene expression. These transgenic lines also contained the reporter construct *Renilla* luciferase (RLuc), the selection marker Blasticidin-S deaminase, and a C-terminal 2×HA epitope tag (*17*). To construct the donor plasmids, PCR-amplified right homology regions (RHR) and BioXP3200 System-synthesized DNA fragments corresponding to the left homology regions (LHR) fused to the re-codonized 3'-end of each target genes, as well as the target specifying guide RNA sequences, were cloned via Gibson assembly into the pSN054 linear vector (*52*). The final constructs were confirmed by restriction digests and Sanger sequencing. Transfections into Cas9- and T7 RNA polymerase-expressing NF54 parasites were carried out by preloading erythrocytes with the donor plasmids as described previously (*53*). Cultures were maintained in 500 nM anhydrotetracycline

(aTc; Sigma-Aldrich 37919) and 2.5 μg/mL of Blasticidin-S (RPI Corp B12150-0.1). Parasite cell lines stably integrating the donor plasmids were monitored via Giemsa smears and RLuc measurements.

Western blotting of cKD parasite lines. PfACG1 and PfEHD cKD parasites were cultured with 50 nM aTc or without aTc to maintain and downregulated protein expression, respectively. Proteins were then extracted after 72 h via saponin lysis and resuspended in lysis buffer that consists of 4% SDS and 0.5% Triton X-114 in 1×PBS. Proteins were separated on Mini-PROTEAN TGX precast gels (4-15% gradient) in tris-glycine buffer, transferred to a polyvinylidene fluoride (PVDF) membrane using the Mini Trans-Blot Electrophoretic Transfer Cell system, and blocked with 100 mg/mL skim milk in TBS/Tween. Membrane-bound proteins were probed with mouse anti-HA (1:3000; Sigma H3663) and rabbit anti-GAPDH (1:5000; Abcam AB9485) primary antibodies, and anti-mouse (1:5000; Thermo Fisher Scientific 62-6520) and anti-rabbit (1:5000; Cell signaling 7074S) horseradish peroxidase (HRP)-conjugated secondary antibodies. Following incubation in SuperSignal West Pico Chemiluminescent substrate (Thermo Fisher Scientific PI34080), protein blots were imaged and analyzed using the ChemiDoc MP System and Image Lab 5.2.0 (Bio-Rad).

cKD proliferation assays. To assess the effect of conditionally perturbing PfACG1 and PfEHD expression on parasite growth, synchronous ring-stage parasites cultured in the presence (50 and 3 nM) or absence of aTc were cultured in triplicate in a 96-well U-bottom plate (Corning 62406-121). Luminescence signals were taken at 0, 72, and 120 h post-invasion using the Renilla-Glo(R) Luciferase Assay System (Promega E2750) and the GloMax Discover Multimode Microplate

Reader (Promega). The luminescence values in the knockdown conditions were normalized to aTc-treated (100% growth) and chloroquine-treated (200 nM) samples (no growth) as controls and results were analyzed using GraphPad Prism (version 8; GraphPad Software).

Compound susceptibility assays with cKD parasite lines. A stock solution of MMV688533 was dispensed into 96-well U-bottom plates and serially diluted in complete medium to yield final concentrations ranging from 0.3-160 nM. Synchronous ring-stage PfACG1 and PfEHD cKD parasite lines as well as a control cell line expressing an aptamer-regulatable fluorescent protein were maintained in the presence (500 nM) or absence of aTc and were distributed into the drug plates. DMSO- and chloroquine-treated samples (200 nM) served as reference controls. Luminescence was measured after 72 h as described above and EC_{50} values were obtained from corrected dose-response curves using GraphPad Prism.

Immunofluorescence assays

Indirect IFA studies were performed in suspension. Cells were fixed in 4% (v/v) formaldehyde (Thermo Fisher Scientific) for 1 h at room temperature. followed by a second fixation step supplementing the 4% formaldehyde solution with 1 mM cysteine and $CaCl_2$ and subsequent incubation overnight at 4 °C. Cells were then permeabilized on ice using 0.05% Triton X-100 in 1×PBS for 5 min. Autofluorescence was quenched using a 50 mM glycine treatment for 10 min. After two washes in 1× PBS the cells were resuspended in 1% (w/v) bovine serum albumin (BSA) in 1×PBS blocking buffer and were then incubated with the appropriate dilution for each primary antibody used (1:200 for rabbit anti-ERD2 (BEI Recourses), anti-PMT (kindly provided by Choukri Ben Mamoun), anti-PDI (mouse anti-PDI (1D3), Enzo Life Sciences), rabbit or mouse

anti-GFP (Takara (Clontech), Roche), rabbit anti-HA antibodies (Sigma), 1:50 for rabbit anti-Rab5A, Rab5C, or Rab11A, rat anti-Rab5B or Rab7 (kindly provided by Gordon Langsley), 1:200 for anti-coronin (kindly provided by Jake Baum), 1:200 for anti-ACP (kindly provided by Geoffrey McFadden), 1:200 for anti-K13 (*22*), 1:200 for anti-PfCRT antibodies (*54*) followed by incubation with corresponding species-specific secondary antibodies (Alexa Fluor 488-, 594- or 647-conjugated goat anti mouse or rabbit antibodies; Thermo Fisher) diluted 1:2000 in 1% BSA in 1× PBS. MitoTracker Red CMXRos (Thermo Fisher) was used to stain mitochondria. HCS LipidTOX Deep Red Neutral Lipid Stain and Nile Red (Invitrogen) were used to stain neutral lipid bodies according to the protocol provided by the manufacturer. Thin blood smears of stained RBCs were prepared on microscope slides and mounted with cover slips using Prolong Diamond Antifade Mountant with DAPI (Thermo Fisher). Parasites were imaged using a Nikon Eclipse Ti-E wide-field microscope equipped with a sCMOS camera (Andor) and a Plan-apochromate oil immersion objective with 100× magnification (1.4 numerical aperture). A minimum of 27 Z stacks (0.2 µm step size) were photographed for each parasitized RBC. NIS-Elements imaging software (Version 5.02, Nikon) was used to control the microscope and camera as well as to deconvolve the images (using 25 iterations of the Richardson-Lucy algorithm for each image) and perform 3D reconstructions (*22*). ImageJ (Fiji) (version 2.0.0-rc-68/1.52 h) was used to crop the images, adjust brightness and intensity, overlay channels and prepare montages.

Evaluation of genotoxicity

Salmonella typhimurium test strains including the mixed strains TA7001 and TA7006 for detection of base-pair substitutions and TA98 strain for detection of frameshift mutations were used for genotoxicity testing (Ames test). MMV688533 was cytotoxic starting at 300 µg/mL in mixed and

TA98 strains in the absence of metabolic activation. Cytotoxicity was also noted in the presence of metabolic activation starting from 100 µg/mL in TA98 strain and from 1000 µg/mL in mixed strains. Under the conditions of the test, MMV688533 was classified as non-mutagenic.

L5178Y and TK6 cells were used for in vitro micronucleus test to investigate the clastogenicity/aneugenicity potential of MMV688533. There was no statistically significant increase in the number of micronuclei as compared to the solvent control with or without metabolic activation. MMV688533 was therefore deemed non-clastogenic/aneugenic.

Pharmacokinetic studies in mice, rats and dogs

Pharmacokinetic studies in mice were performed following a single intravenous (3 mg/kg) or oral (3.5, 10 and 30 mg/kg) administration of MMV688533 to male Swiss mice (3 dosed intravenous (i.v.) and 3 per os (p.o.)). Feeding was performed *ad libitum*. Vehicles / Formulations were at 0.6 mg/mL in PEG200/Solutol/G5% (20%/5%/75%) for i.v. solution and at 0.3, 1 and 3 mg/mL in Methylcellulose /Tween 80 (0.6%/0.5%) for p.o. suspensions in water. Administration modes were i.v. 3 mg/kg, 5 mL/kg and p.o. 3.5, 10 and 30 mg/kg,10 mL/kg. Matrix and Sampling times were for i.v. plasma and lung / 0.083, 0.5, 1, 2, 4, 6, 8 and 24 h and for p.o plasma (only at 10 mg/kg), blood, liver and lung / 0.25, 0.5, 1, 2, 4, 6, 8 and 24 h. The analytical method was LC-MS/MS with a lower limit(s) of quantification 2 ng/mL for plasma, 5 ng/mL for blood and 6 ng/g for tissues. PK analysis were performed using non-compartmental models (Plasma, IV bolus and Plasma, Extravascular) Phoenix (WinNonLin version 6.4).

In rats, the PK studies were performed following a single intravenous (3 mg/kg) or oral (10 mg/kg) administration to male Sprague-Dawley rats. The procedure was as described above but for the following exception: The rats were not fasted and the oral volume of administration of 10 mg/kg was 10 mL/kg Matrix. The sampling times for i.v. blood were 0.083, 0.25, 0.5, 1, 2, 4, 7, 24 and 48 h and for p.o. blood 0.5, 1, 2, 4, 7, 24 and 48 h. PK analysis was performed using a the 200-202, IV bolus and Extravascular non-compartmental models.

In dogs, the PK of MMV688533 was performed following a single 2 mg/kg intravenous administration of the compound to female Beagle dogs that were fasted overnight. The vehicle / formulation solution was at 2 mg/mL PEG400/Ethanol/Solutol HS15/G5 % (20/5/5/70) pH 3. For administration, i.v. was the preferred route (2 mg/kg, 1 mL/kg). Matrix and sampling times were blood at 0.083, 0.25, 0.5, 1, 2, 4, 6, 8, 24, 30, 48 and 72 h. The limit of quantification was 1 ng/mL. MMV688533 following a single oral dose of 0.5 mg/kg was also administered as malonate salt in a capsule or oral solution to male Beagle pentagastrin-dogs weighing 8.6 to 10.8 kg. 3 males per dose were dosed p.o, and serial sampling was applied. Feeding conditions were fasted overnight and fed 4 h post dosing. Vehicles / Formulations were capsule (MMV688533/microcrystalline cellulose/ croscarmellose sodium (5/91.67/3.33) followed by 50 mL of water. Solution at 0.25 mg/mL in PEG400/Ethanol/Solutol/G5% (20/5/7.5/67.5). Administration mode was p.o. 0.5 mg/kg (active compound), 2 mL/kg for solution. Matrix and sampling times were blood at 0.25, 0.5, 1, 2, 4, 6, 24, 48, 72 and 168 h. Limit of quantification was 0.833 ng/mL for MMV688533.

Safety pharmacology profiling

Preliminary non-clinical toxicology studies in rats. Two-week toxicity studies in rats were conducted to evaluate the potential toxicity of MMV688533 (malonate form) when administered once daily for 15 days to Sprague Dawley rats by the oral route (gavage). Four study groups, each composed of 5 male and 5 female Sprague Dawley rats, were given MMV688533 at 12.5, 25 or 50 mg/kg/day or vehicle alone [0.5% (w/w) Polysorbate 80 and 0.6% (w/w) methylcellulose in water], once daily for 15 consecutive days, under a dose-volume of 5 mL/kg. In addition, 3 satellite rats/sex/group were included in the study. These rats received the test item in the same conditions as principal animals and were used for toxicokinetic studies. Parameters evaluated included mortality, clinical signs, body weight, and food consumption. Blood samples for hematology, coagulation and clinical chemistry were collected from all principal animals on day 3 and at necropsy. Blood samples for toxicokinetic determinations were obtained from satellite animals at 1, 2, 4, 7 and 24 h after dosing on day 1, as well as 1, 2, 4, 7, 24, 48 and 96 h after dosing on day 14. Control animals were sampled at 4 and 24 h after dosing on both days. At necropsy, all study animals were observed for any macroscopic post-mortem examinations, and weights of selected organs were recorded. Representative tissue samples at 50 mg/kg/day and in controls were histologically examined. Tissues with suspected compound-related microscopic findings were also evaluated microscopically for rats in the lower dose groups.

Preliminary non-clinical toxicology studies in dogs. Two male and two female beagle dogs were given MMV688533 (malonate form) at 10, 30 or 100 mg/kg/day, or the vehicle alone [0.5% (w/w) Polysorbate 80 and 0.6% (w/w) methylcellulose in water], once a day for 15 consecutive days, under a dose-volume of 5 mL/kg. Animals of all groups were treated for 15 days, except for those at 100

mg/kg/day, which were euthanized prematurely after 11 and 10 administrations, respectively for males and females, for ethical reasons. Parameters evaluated included mortality, clinical signs, body weights and food consumption. Blood samples for hematology, coagulation and clinical chemistry analyses were collected once during the pretest period and on Days 3 and 8 (all animals), and on Day 14 (groups 1, 2 and 3). Urine samples for chemistry analyses were collected once during the pretest period (all animals) and on Day 14 (groups 1, 2 and 3). At necropsy [Day 10 (group 4 females) or 11 (group 4 males), or Day 16 for group 1, 2 and 3 animals], all study animals were observed for any macroscopic post-mortem examinations, and weights of selected organs were recorded and representative tissue samples were examined. In addition, the toxicokinetic profiles of MMV688533 and its main metabolite MMV893023 were determined from blood samples collected on Day 1 (all animals) and on Day 15 (groups 1, 2 and 3) at 1, 2, 4, 7 and 24 hours post-dosing. For group 4 animals, blood samples for TK determinations were collected on Day 11 for the males or on Day 10 for the females, before dosing, and 1 and 2 hours post-dosing.

Ex vivo rabbit Purkinje fibers cardiovascular study. This study was designed to evaluate the cardiac cellular electrophysiological effects of MMV688533 on the action potential parameters in isolated rabbit Purkinje fibers. MMV688533 was tested at 0.1, 1.4, 4.9 and 6.4 µmol/L corresponding to 0.05, 0.7, 2.5 and 3.3 µg/mL of active ingredient, respectively. The effects of the active MMV688533 metabolite RA11263363A on resting membrane potential and action potential parameters recorded from isolated rabbit Purkinje fibers (male, New Zealand rabbits; 1.3 to 1.5 kg; 7-10 weeks of age) were evaluated through a microelectrode technique. The following parameters were measured: resting potential (RP in mV), amplitude (APA in mV), maximal rate of rise of action potential (Vmax in V/s) and the action potential duration at 50 and 90% of repolarization (APD50 and APD90 in ms).

The fibers were superfused with an oxygenated physiological solution containing 120 mM NaCl; 4 mM KCl; 1 mM $MgCl_2$; 1.8 mM NaH_2PO_4; 25 mM $NaHCO_3$; 11 mM glucose; 1.8 mM $CaCl_2$; pH = 7.4, at 36±1°C. RA11263363A (592.3 g/mol, salt form and 519.4 g/mol, base form, batch CLT.CBN1.039.1) was first dissolved into DMSO to obtain a 12 mM stock solution. This solution was further diluted with 100% DMSO to obtain solutions at 4, 1.2 and 0.12 mM. These four solutions (0.12, 1.2, 4 and 12 mM) were added into the physiological solution to obtain the appropriate nominal concentrations of 0.3, 3, 10 and 30 µM, which corresponded to 0.2, 1.6, 5.2 and 15.6 µg/mL of active ingredient respectively. The final concentration of DMSO in the test formulation was kept constant at 0.25% (v/v) in the physiological solution. Purkinje fibers (n=3) were first superfused by the physiological solution. After a 30-minute control period, test compound was evaluated at increasing concentrations sequentially applied, every 30 minutes. For each tested concentration, the fibers were stimulated at the basal rate of 1 pulse per second (1 Hz). In addition, stimulation rate was decreased from 1 pulse per second (1 Hz) to 1 pulse every 4 seconds (0.25 Hz) for 3 minutes, increased again to 1 pulse per second for 1 minute and finally increased to 3 pulses per second (3 Hz) for 2 additional minutes (between the 19th and the 25th minute). The low stimulation rate was used to favor the occurrence of abnormal electrical events during the repolarization phase of the action potential and to facilitate the development of Early After Depolarization's (EADs). The high stimulation rate was used to evaluate the use-dependent sodium channel blockade. After the highest concentration, the physiological solution was superfused again to evaluate the reversibility of the drug effect (washout).

In vivo ***anaesthetized guinea pig cardiovascular study.*** The purpose of this study was to assess the potential effects on cardiovascular parameters of continuous intravenous (IV) administration of MMV688533 chlorhydrate to anesthetized guinea pigs, when tested at cumulative doses of 10, 20

and 30 mg/kg. Each dose was successively administered as a 15-min infusion/dose. Blood concentrations of MMV688533 were also assessed. An aqueous solution of ethanol/solutol/NaCl (10% / 5% / 85%, v/v/v) was used for the study. Cardiovascular functions were evaluated by measuring hemodynamic parameters like arterial blood pressure (BP) and heart rate (HR), and electrocardiographic (ECG) parameters.

Animals were premedicated with buprenorphine (0.05 mg/kg intramuscular) ~30 min prior to surgery and anesthesia maintained under isoflurane (2-5%) and constant O_2 flux (0.7 – 1.3 mL/min). Under deep anesthesia, lidocaine was injected subcutaneously at sites of the tracheotomy and insertion of electrocardiogram needles, and a tracheotomy performed to allow mechanical ventilation followed by carotid (arterial measurements) and jugular (infusion of control article or test article) catheterizations. Administration of Ringer lactate solution (5 mL/ kg intraperitoneal), heated to body temperature to compensate for the hydric loss inherent to anesthesia, was performed at the discretion of the study director according to major bleeding surgery or signal instability (information documented in study records). BP and ECG parameters were recorded in anesthetized guinea pigs placed on a heating pad. Systemic BP was recorded using an independent catheter pressure transducer (MillarTM equipment) introduced into the carotid artery. The standard ECG (one lead derivation among L1 or L2 or L3) was recorded using four subcutaneously-placed needle electrodes to provide an optimal separation of T wave from P wave of the next complex. Once satisfactory in terms of their quality and stability, the signals were recorded for 15 minutes (corresponding to the stability period). Thereafter a set of animals (group T2) received a NaCl infusion (starting at T0 min) followed by RA11263363A at cumulative doses of 10, 20 and 30 mg/kg. Each infusion was delivered every 15 minutes at a rate of 0.3 mL/kg/min, with the last infusion followed by a period of recovery.

At the end of the recovery period (T75 min) one single arterial blood sample (~0.2 mL) was collected from the abdominal artery. A second set of animals (group T1) was infused with the control article in the same experimental conditions without the terminal blood sampling. A last set (group T3) was dedicated to evaluating pharmacokinetic (PK) parameters in which animals fitted with a jugular catheter (for RA11263363A infusion) and a carotid catheter (arterial blood sampling) were treated in the same experimental conditions as those described for the group T2. At the end of each 15-min period of infusion a blood sample (~0.2 mL) was collected. This was also done during the recovery period at 5, 10 and 75 min. Each volume of blood collected was immediately replaced by an equivalent volume of Ringer lactate solution. Of note, in group T3, at the end of the recovery period (T75 min) arterial blood (~0.2 mL) was sampled and was compared to the corresponding sample in group T2. All blood samples (0.2 mL) were collected with sodium heparinate as anticoagulant and placed on wet ice immediately after collection. Then all samples were stored at -20°C until analysis. Thereafter the animals were euthanized by IV or intra-cardiac overdose of sodium pentobarbital.

Patch Clamp electrophysiological hERG assay

Cell culture procedure. HEK293 cells were stably transfected with hERG cDNA. Stable transfectants were selected by co-expression with the Geneticin (G418)-resistance gene incorporated into the expression plasmid. Selection pressure was maintained by including G418 in the culture medium. Cells were cultured in Dulbecco's Modified Eagle Medium / Nutrient Mixture F-12 (D-MEM/F-12) supplemented with 10% fetal bovine serum, 100 U/mL penicillin G sodium, 100 µg/mL streptomycin sulfate and 500 µg/mL G418.

Electrophysiological Procedures. Cells were transferred to the recording chamber and superfused with vehicle control solution. Micropipette solution for whole cell patch clamp recordings was composed of: 130 mM potassium aspartate; 5mM $MgCl_2$; 5mM EGTA; 4mM ATP; 10mM HEPES. The pH was adjusted to 7.2 with KOH. Micropipette solution was prepared in batches, aliquoted, frozen for storage and a fresh aliquot thawed each day. The recording was performed at a temperature of 33-35 ºC using a combination of in-line solution pre-heater, chamber heater and feedback temperature controller. Temperature was measured using a thermistor probe in the recording chamber. Micropipettes for patch clamp recording were made from glass capillary tubing using a P-97 (Sutter Instruments, Novato, CA) or PC-10 (Narshige, Amityville, NY) micropipette puller. A commercial patch clamp amplifier (PC-505B from Warner Instruments, Hamden CT) was used for whole cell recordings. Before digitization, current records were low-pass filtered at one-fifth of the sampling frequency.

Experimental Procedures. Cells stably expressing hERG were held at -80 mV. Onset and steady state inhibition of hERG potassium current due to MMV688533 were measured using a pulse pattern with fixed amplitudes (conditioning prepulse +20 mV for 1 s; repolarizing test ramp to -80 mV (-0.5 V/s) repeated at 5 s intervals). Each recording ended with a final application of a supramaximal concentration of the reference substance (E-4031, 500 nM) to assess the contribution of endogenous currents. The remaining uninhibited current was subtracted off-line digitally from the data to determine the potency of the test substance for hERG inhibition. MMV688533 was tested at 1 μM in three cells (n = 3). Inhibitory effects on hERG potassium current amplitude of 17.9, 11.5 and 12.4% were observed. Based on these results and the solubility limit of the test article in the vehicle, additional nominal concentrations (0.3 and 3 μM; Protocol Amendment No. 1) were selected to

evaluate the concentration-response relationship. One or more test article concentrations were applied sequentially (without washout between test substance concentrations) in ascending order, to each cell ($n \geq 3$). Peak current was measured during the test ramp. A steady state was maintained for at least 20 s before applying test article or positive control. Peak current was measured until a new steady state was achieved.

Supplementary Figures

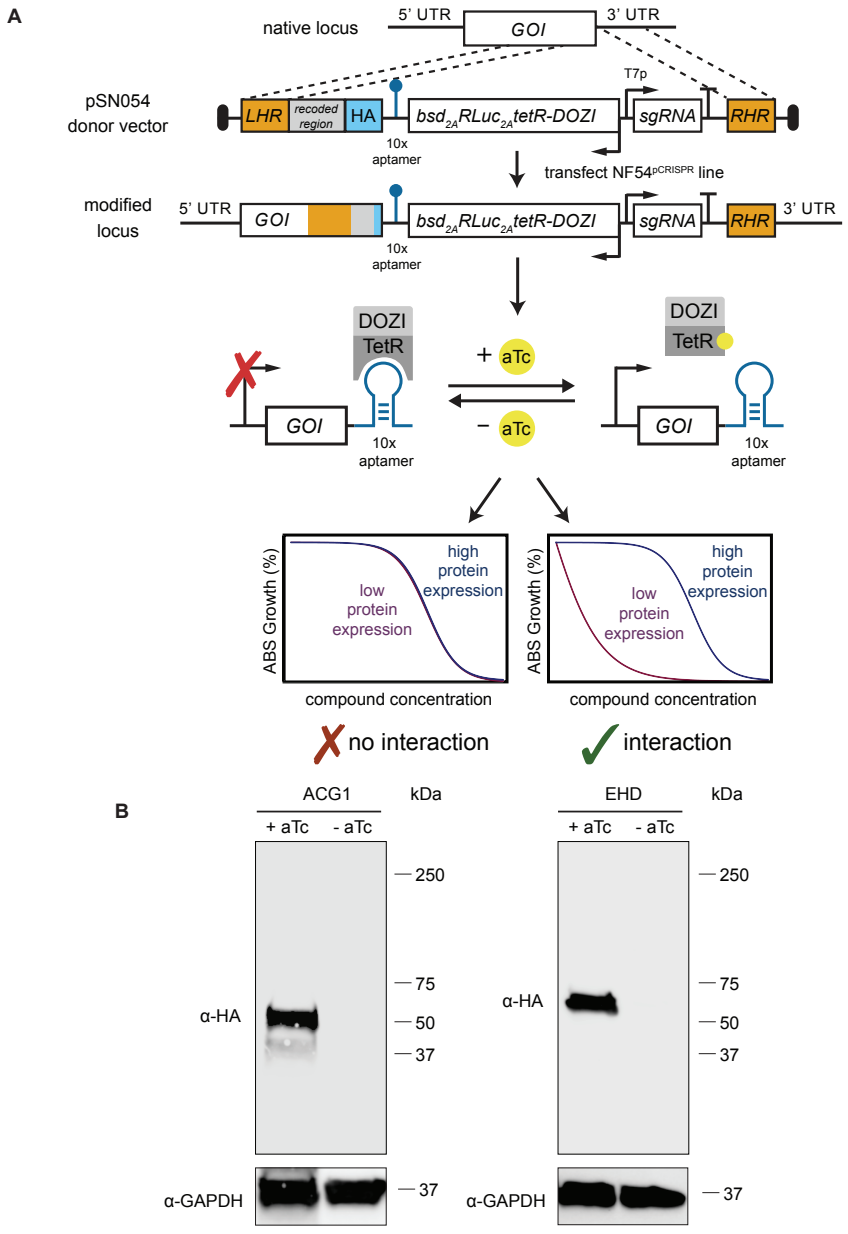

Fig. S1. Conditional knockdown (cKD) strategy for PfACG1 and PfEHD. (A) Schematic representation of the generation of PfACG1 and PfEHD cKD lines. **(B)** Western blot-based assessment of PfACG1 and PfEHD translational regulation via the TetR-DOZI-RNA aptamer module. The expected mass of the PfACG1-2×HA and EHD-2×HA proteins is 55.7 kDa and 66.4 kDa, respectively. Protein expression was maintained in the presence of aTc, contrasting with undetectable levels of either protein upon aTC removal. GAPDH was a loading control.

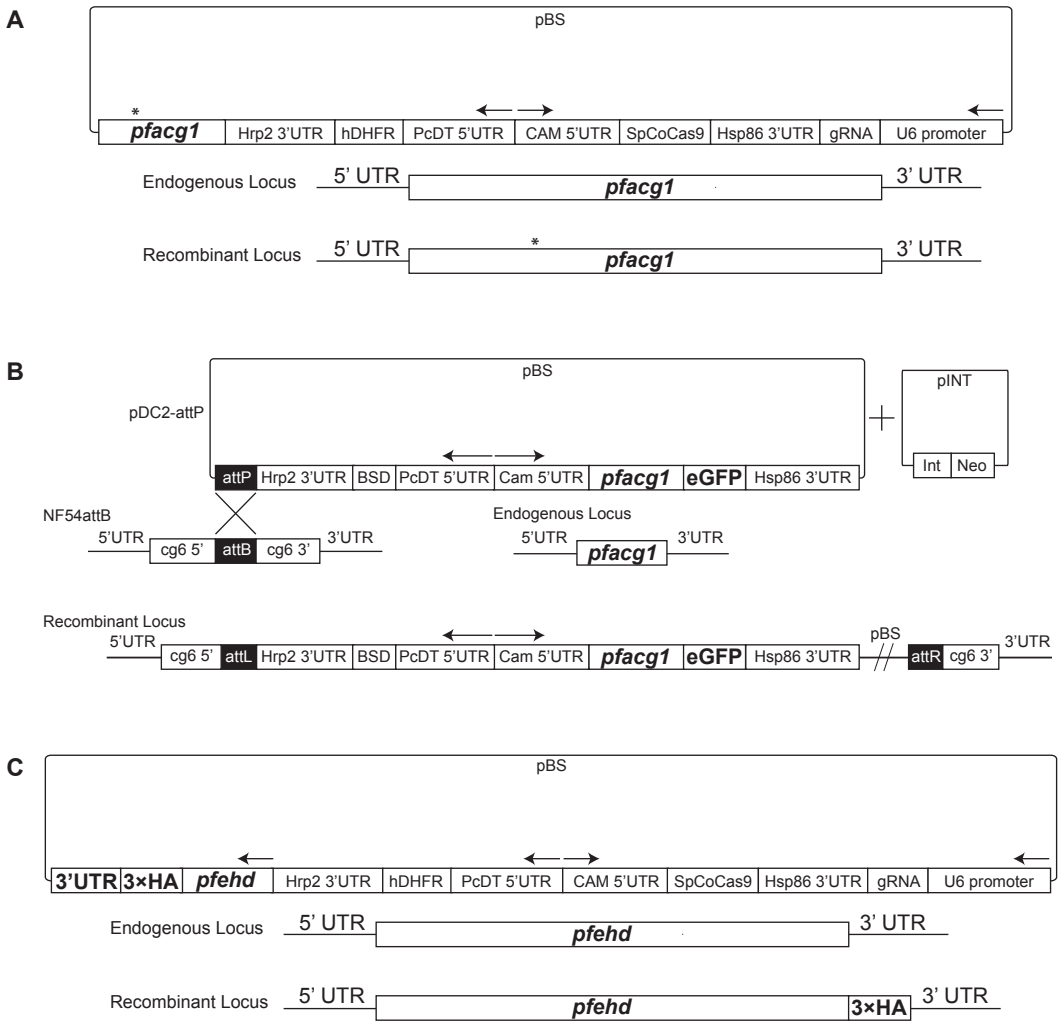

Fig. S2. Genetic manipulation strategies for PfACG1 and PfEHD. (A) CRISPR/Cas9 strategy to edit SNPs into the endogenous *pfacg1* locus. Cas9 was derived from *Streptococcus pyogenes* and codon optimized for *P. falciparum*; transcription was regulated from a *P. falciparum* calmodulin promoter. The plasmid also contains a hDHFR selectable marker under the PcDT promoter and a sequence encoding the guide RNA (gRNA) under a U6 promoter. The *pfacg1* donor has >300bp of homology flanking the mutation of interest (G96V or W286R). **(B)** attB×attP based strategy to integrate *pfacg1*-eGFP as a transgene into the *cg6* locus of NF54attB parasites. *pfacg1*-eGFP and the BSD selectable marker are transcribed from a calmodulin and a PcDT promoter, respectively. **(C)** CRISPR/Cas9 strategy to introduce a 3×HA into the 3' end of the endogenous *pfehd* locus in NF54attB parasites expressing the *pfacg1*-eGFP transgene. The plasmid also contains a hDHFR selectable marker and a sequence encoding the guide RNA

(gRNA), under a PcDT and a U6 promoter, respectively. The donor fragment has two regions of *pfehd* homology flanking the 3×HA tag. attL: attB left junction segment; attR: attB right junction segment. BSD: Blasticidin-S deaminase; CAM: Calmodulin; eGFP: enhanced Green Fluorescent Protein; gRNA: guide RNA. hDHFR: human dihydrofolate reductase; Hrp2: histidine-rich protein 2; Int: Mycobacteriophage Bxb1 serine integrase; Neo: Neomycin; pBS: BlueScript plasmid; Hsp86: Heat shock protein 86; PcDT: *Plasmodium chabaudi* dihydrofolate reductase-thymidylate synthase; *pfacg1*: *Plasmodium falciparum* acylguanidine 1 gene; *pfehd: Plasmodium falciparum* Eps15 homology domain containing gene; SpCoCas9: *Streptococcus pyogenes-Plasmodium falciparum* codon-optimized Cas9; UTR: Untranslated region.

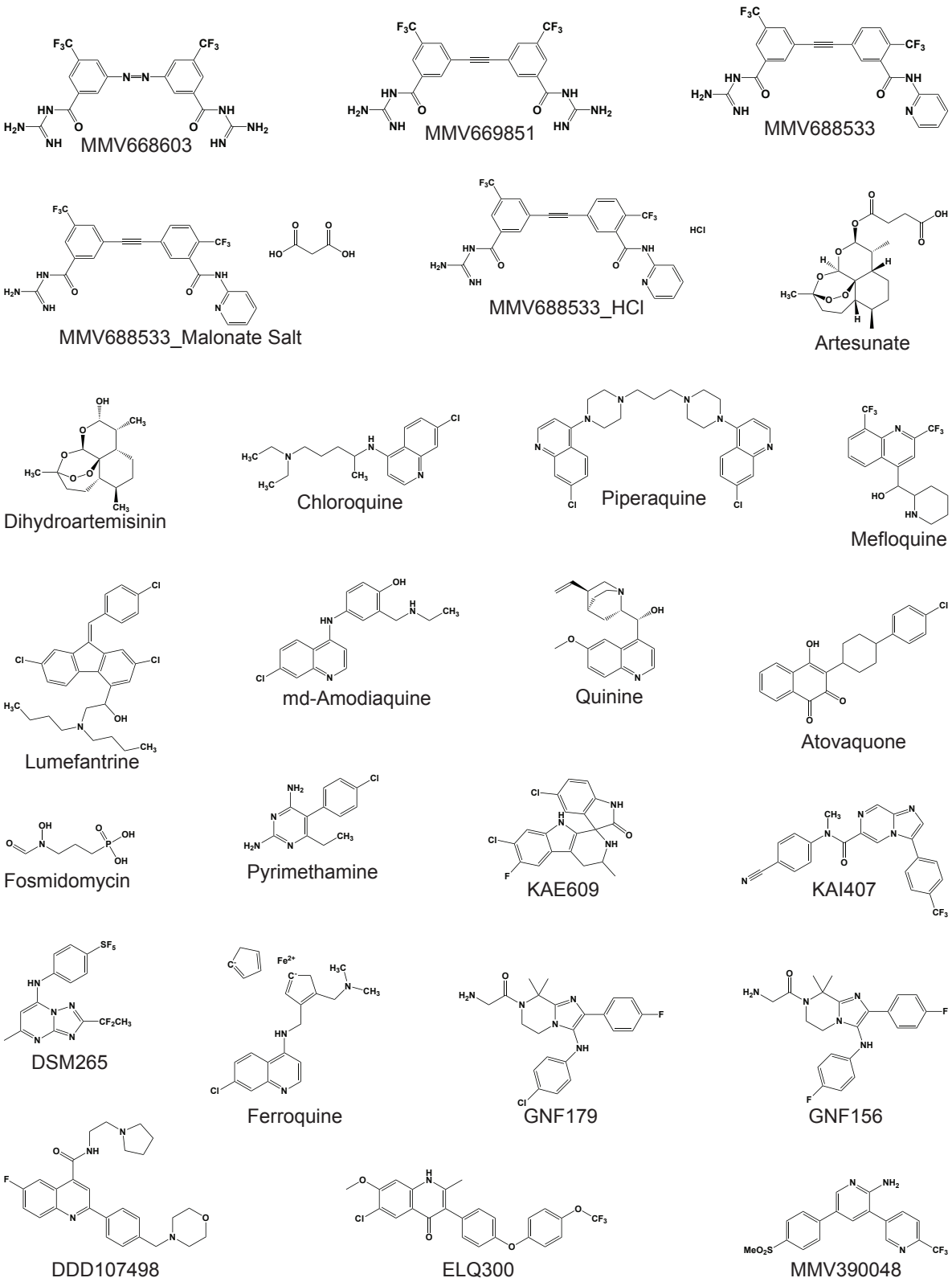

Figure S3. Chemical structures of antimalarial compounds tested herein.

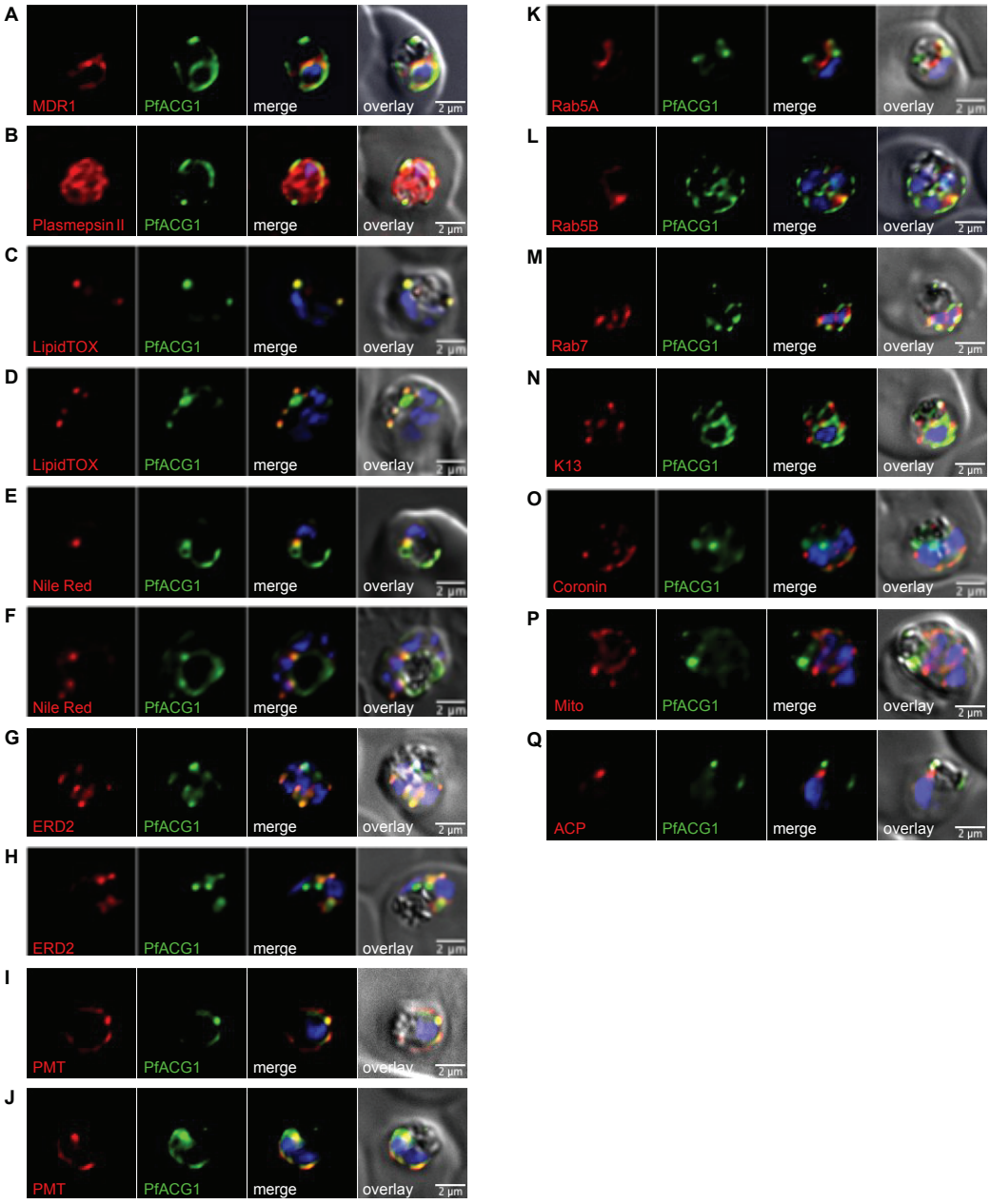

Fig. S4. Fluorescence microscopy images of fixed and labeled NF54$^{3\times HA\text{-}EHD}$attB-ACG1-eGFP parasites. PfACG1 was detected using antibodies specific to eGFP. Costaining used **(A)** anti-PfMDR1 antibodies that label the digestive vacuole membrane (*55, 56*); **(B)** anti-plasmepsin II antibodies that label the digestive vacuole lumen (*57*); **(C, D)** LipidTOX neutral lipid stain that stains lipid bodies (*58*); **(E, F)** Nile Red that also stains lipid bodies (*59*); **(G, H)** anti-ERD2 antibodies that label the cis-golgi (*19*); **(I, J)** anti-PMT that labels phosphoethanolamine N-methyltransferase present in trans-Golgi structures (*20*); **(K-M)** anti-Rab5A, anti-Rab5B and anti-Rab7 that labels vesicles (*22*); **(N)** anti-K13 that labels the ER, vesicles and cytostomes (*22*); **(O)** anti-coronin antibodies that stain compartments with F-actin (*60*); **(P)** MitoTracker Red that labels mitochondria; or **(Q)** anti-ACP antibodies that label the acyl carrier protein present in the apicoplast (*61*). Nuclei were stained with DAPI (blue). Scale bars: 2 µm.

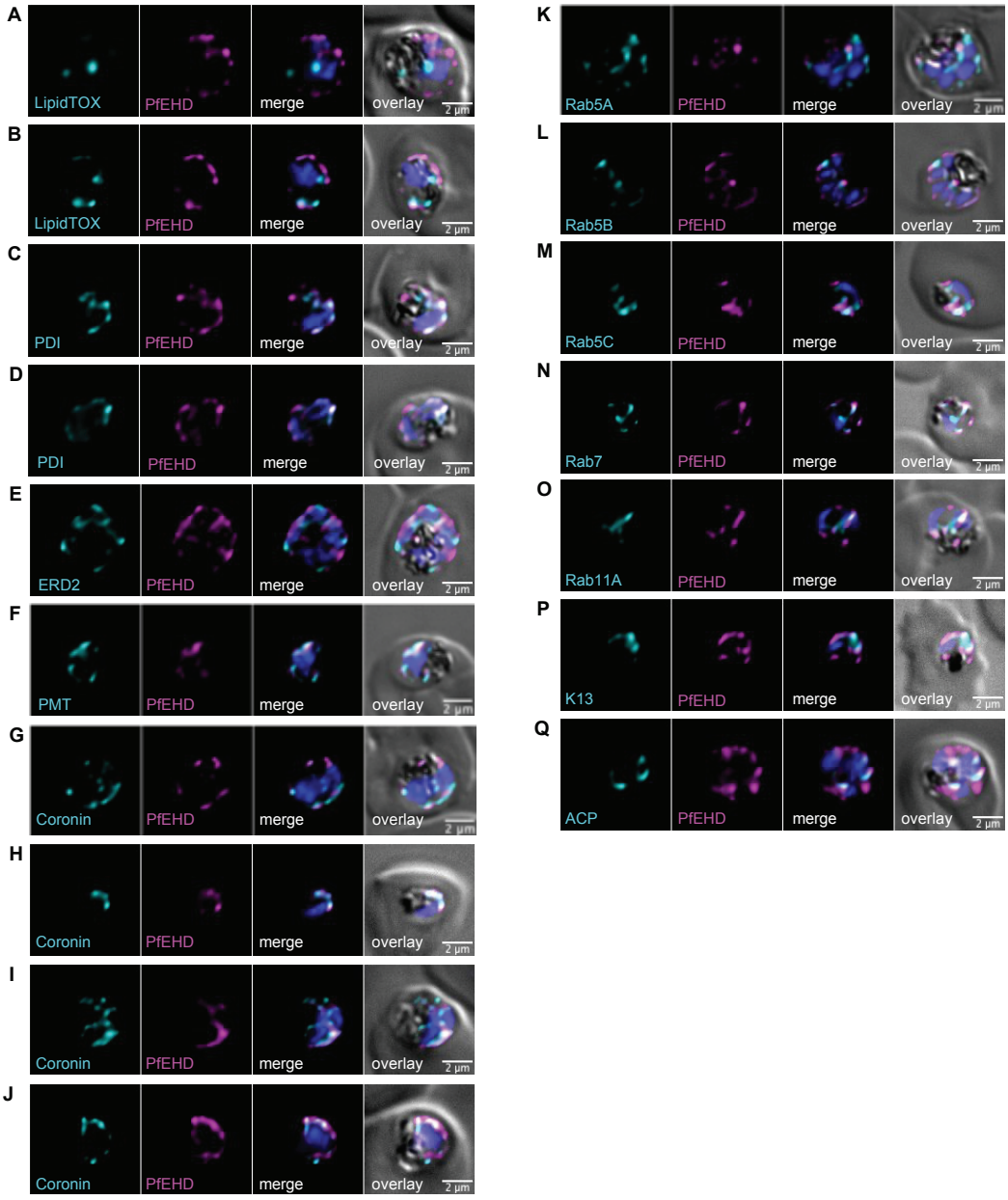

Fig. S5. Fluorescence microscopy images of fixed and labeled NF54$^{3\times HA\text{-}EHD}$attB-ACG1-eGFP parasites. PfEHD was detected using antibodies specific to HA (magenta). Costaining used **(A, B)** LipidTOX neutral lipid stain; **(C, D)** anti-PDI that labels the plasmodial protein disulfide isomerase that is localized in the ER (*62*); **(E)** anti-ERD2; **(F)** anti-PMT; **(G-J)** anti-coronin; **(K-0)** anti-Rab5A, anti-Rab5B, anti-Rab5C, anti-Rab7 and anti-Rab11A that label vesicles involved in trafficking (*63, 64*); **(P)** anti-K13; or **(Q)** anti-ACP antibodies (cyan). Nuclei were stained with DAPI (blue). Scale bars: 2 µm.

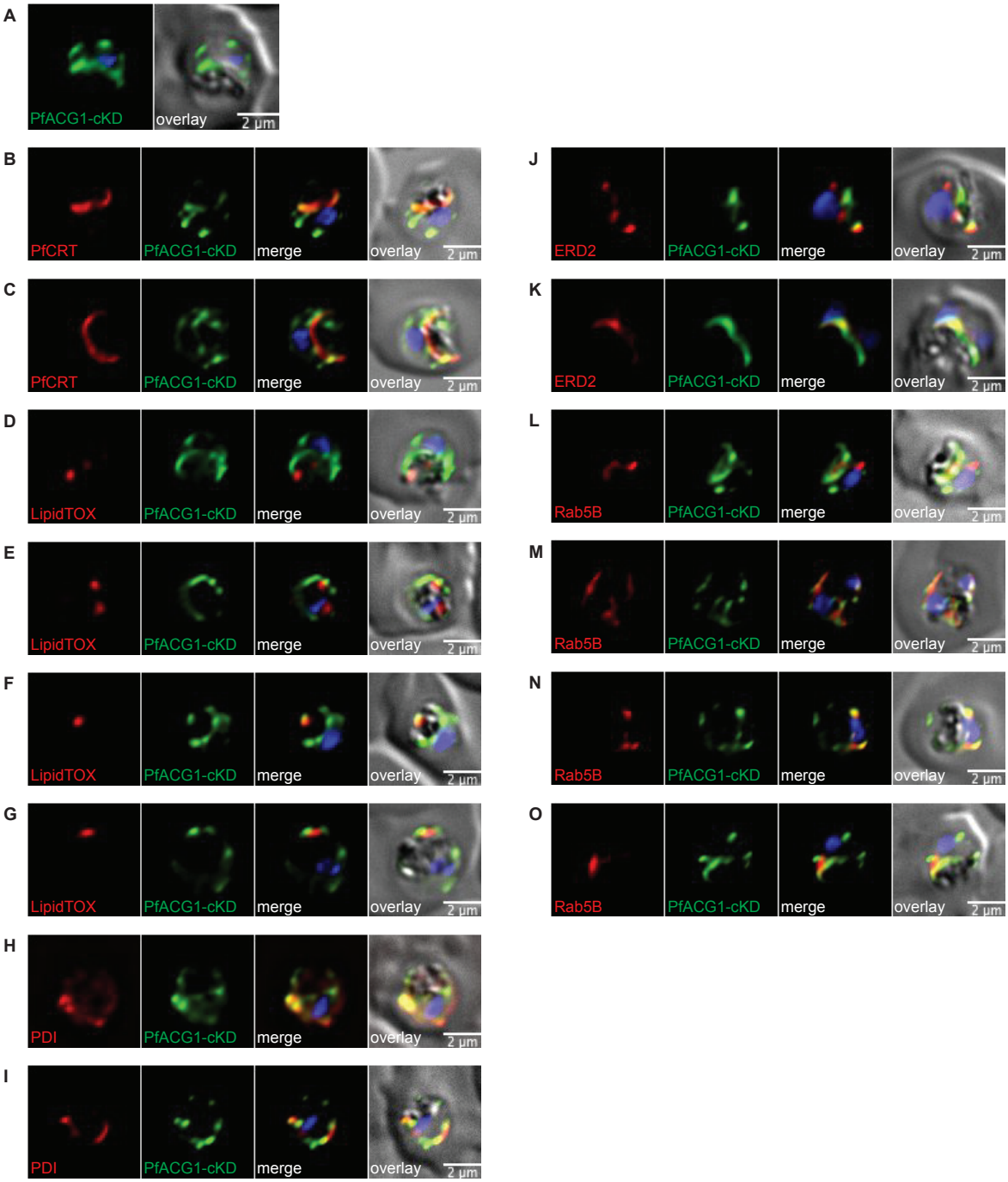

Fig. S6. Fluorescence microscopy images of fixed and labeled NF54^{pCRISPR}TetR-DOZI-ACG1-2×HA parasites. PfACG1 was detected using antibodies specific to HA (green). Costaining used **(A)** anti-HA stain; **(B-C)** anti-PfCRT antibodies that label the digestive vacuole membrane (*65*); **(D-G)** LipidTOX neutral lipid stain; **(H-I)** anti-PDI; **(J-K)** anti-ERD2; **(L-0)** anti-Rab5B. Nuclei were stained with DAPI (blue). Scale bars: 2 µm.

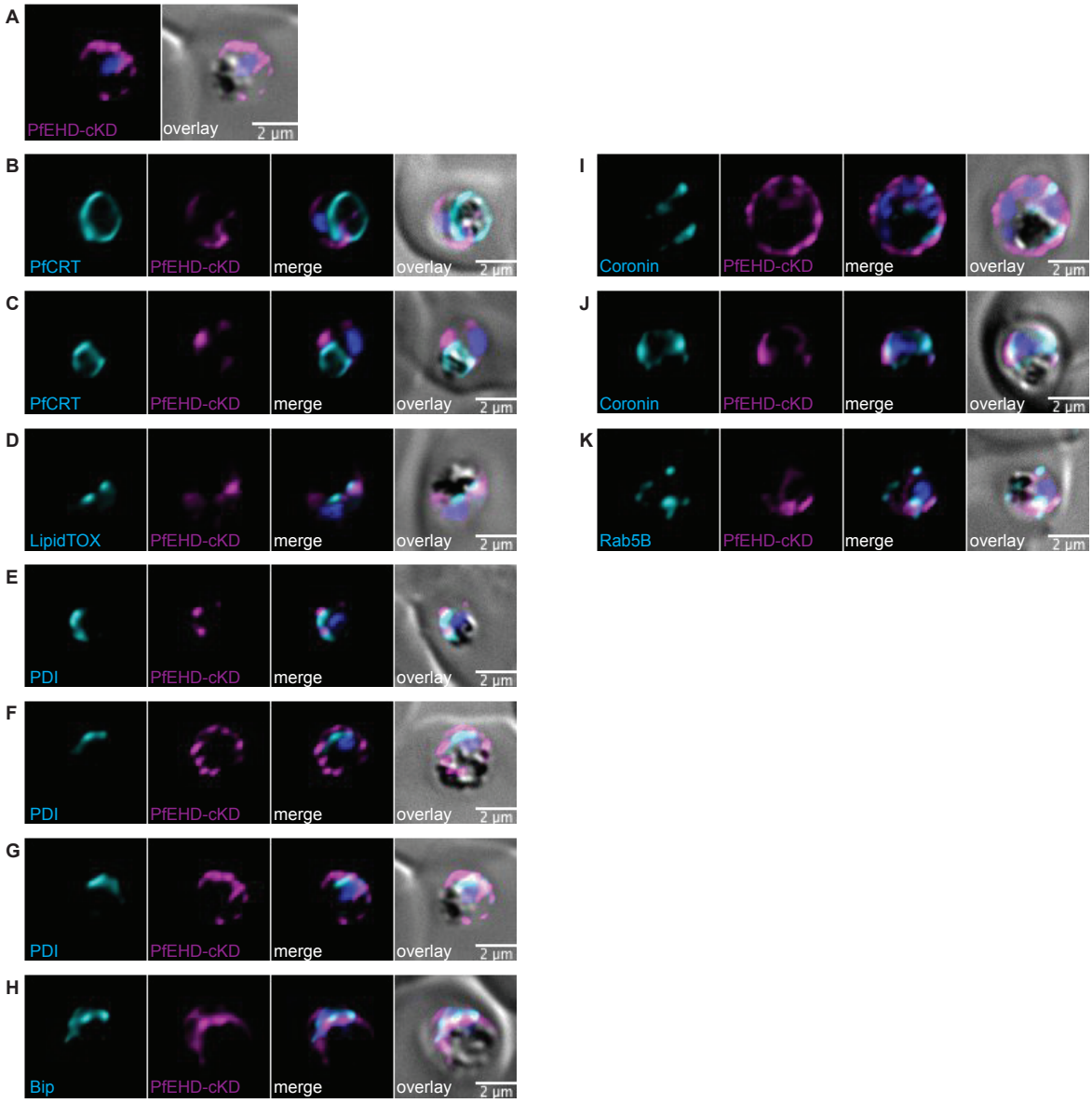

Fig. S7. Fluorescence microscopy images of fixed and labeled NF54^{pCRISPR}TetR-DOZI-EHD-2×HA parasites. PfEHD was detected using antibodies specific to HA (magenta). Costaining used **(A)** anti-HA stain; **(B-C)** anti-PfCRT; **(D)** LipidTOX neutral lipid stain; **(E-G)** anti-PDI; **(H)** Bip antibodies that stain the ER (*20*); **(I-J)** anti-coronin; **(K)** anti-Rab5B. Nuclei were stained with DAPI (blue). Scale bars: 2 µm.

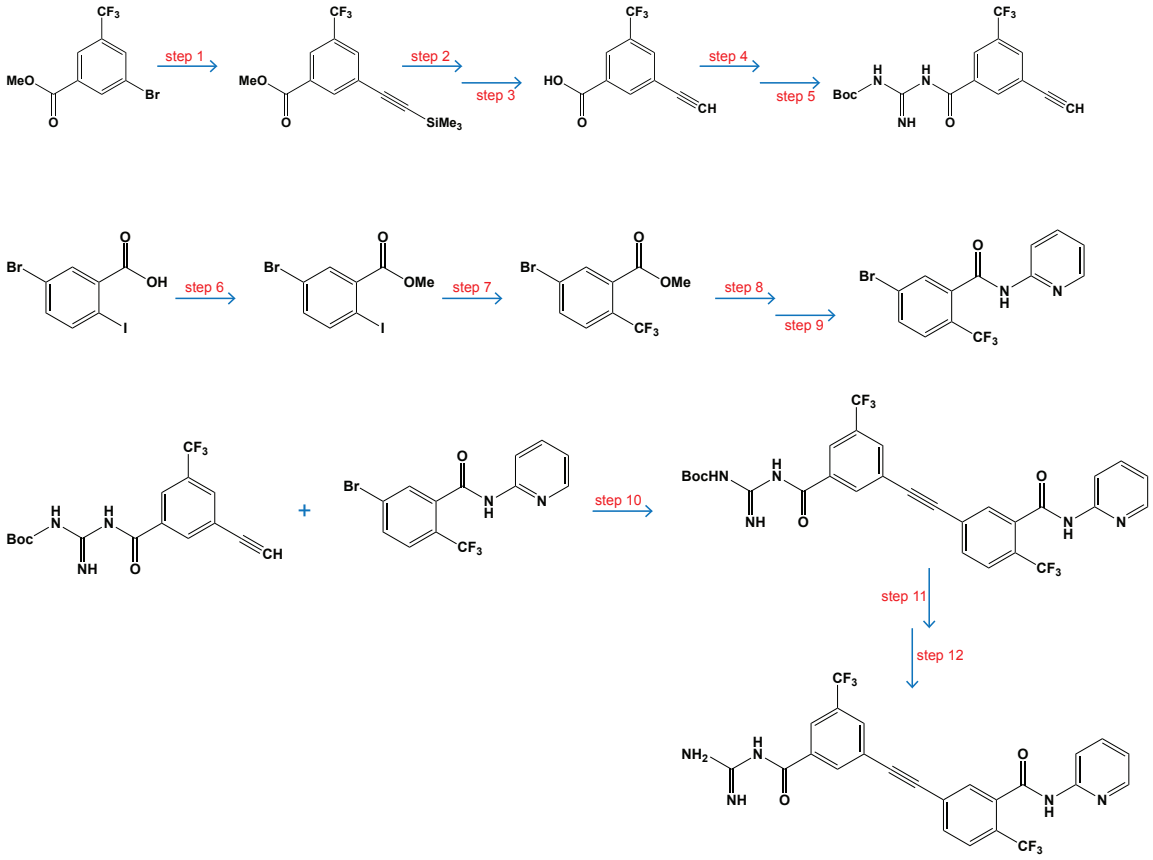

Fig. S8. MMV688533 synthesis.

Supplementary Tables

Table S1A. MMV688533 chemical formula and calculated /experimental properties of malonate salt.

Chemical name	5-[2-[3-(carbamimidoylcarbamoyl)-5-(trifluoromethyl)phenyl]ethynyl]-N-(2-pyridyl)-2-(trifluoromethyl)benzamide, malonate salt
Molecular weight	623.47 g/mol (free base: 519.41 g/mol)
Molecular formula	$C_{27}H_{19}F_6N_5O_6$ (free base: $C_{24}H_{15}F_6N_5O_2$)
Rings	3
Hydrogen bond donor	5
Hydrogen bond acceptor	7
tPSA (Å)	195.03 (free base: 120.43)
Number of chiral centers	0
pK_a (measured)	2.4 (base) /5.8 (base)
LogP (calculated/measured)	3.93 / No value (> 3)*
LogD (pH.4)	3.79
Polymorphism	All batches synthetized so far are under the same crystalline form (anhydrous form)
Melting point	180°C

* Technical limit of the Syrius T3 apparatus. tPSA: Topological polar surface area (the sum of the surface of all polar atoms, primarily oxygen and nitrogen including hydrogen atoms). Compounds with tPSA >140 Å suffer from poor cell permeability. pKa: Dissociation constant. LogP: Partition coefficient. LogD: Distribution coefficient. LogP is expressed as a log10 of the concentration ratio between non-aqueous organic (n-octanol) and aqueous (pH-buffered water). Ideally, compounds should possess a LogP value not greater than 5 (otherwise too lipophilic, thereby creating solubility issues). LogD is a distribution coefficient related to the lipophilicity of ionizable compounds (pH dependent).

Table S1B. MMV688533 (malonate salt) solubilization profile against time.

MMV688533	Solubility µg/mL						pH		X-Ray diffraction results at 24 hr	Predicted solubility of malonate salt
	Room temperature									
Time (hours)	0.25	0.5	1	2	4	24	Medium	Supernatant (24h)		
pH 1.0 (0.1N HCl)	1750	2480	2870	2670	3770	4780	1.1	1.1	Malonate form1	≥ 4.7 mg/ml
pH 3.0	2.8	5.4	6.5	7.6	7.2	14.2	2.8	2.9	Malonate form1	≥ 14 µg/ml
pH 4.5	1.6	2.1	2.72	3	2.8	0.96	4.3	4.3	Malonate form1	≤ 3 µg/ml
pH 7.4	<LOQ	<LOQ	<LOQ	<LOQ	<LOQ	<LOQ	7.4	6.5	Base form 2	≤ 3 µg/ml
Water	1	2	4.3	7.6	10	14.4	N/A	3.1	Malonate form1	
	37°C									
Gastric fasted state	4220	3540	1890	1670	1010	420	1.3	1.5	Salt probably monohydrochloride	≥ 4.2 mg/ml
Gastric fed state	11	12	14	15	18	27	3.1	3.1	Malonate form1	27 µg/ml
Fasted state simulated intestinal fluid	107	154	15	11	13	20	6.7	4.7	Base form2	≥ 150 µg/ml
Fed state simulated intestinal fluid	3980	3540	1760	1990	2180	150	5	4.8	Base form2	≥ 3.9 mg/ml

The equilibrium solubility of MMV688533 malonate salt in buffered solutions (room temperature) and physiological relevant aqueous buffers (37°C) is pH dependent. Good solubility was observed in acidic conditions and poor solubility under more neutral conditions. Because the solubility of malonate salt is difficult to assess in some media due to its conversion into the free base form 2 (hydrated form of free base), we determined the concentration of solubilized compound as a function of time. LOQ: Limit Of Quantification. Low solubility is < 10 µg/mL; moderate solubility is between 10 µg/mL and 1000 µg/mL; high solubility is > 1000 µg/mL.

Table S1C. MMV688533 in vitro IC_{50} (nM) of culture-adapted lab and field *P. falciparum* isolates.

Salt	NF54	3D7	K1	Dd2	HB3	7G8	TM90C2B	D6	V1/S	FCB	Cam3.1	PFeEF2 Y186N	PFDXR CNV	PFPI4K S743T	PFCARL I1139K	PFDHOD H G181C	PFCYTB I22L
HCl	9.0	8.6	7.3	7.8	2.5	5.5	4.1	4.4	7.1	8.5	-	7.5	8.7	7.2	7.3	-	-
Malonate	16	31*	-	-	-	-	15	-	-	-	16	-	-	15	-	21	18

MMV688533 potency on chloroquine-sensitive (NF54, 3D7) and chloroquine-resistant (K1, Dd2) parasites, as determined from dose-response assays and IC_{50} analyses, was below 10 nM. This compound showed no cross-resistance with other known antimalarials as determined using a diverse panel of lab-adapted field isolates: HB3, 7G8, TM90C2B, D6, V1/S, FCB and Cam3.1. No cross resistance was observed with Dd2 mutant parasites selected for resistance to DDD107498, fosmidomycin, MMV390048, GNF156, DSM265 or ELQ300 and which acquired resistance via amino acid substitutions or copy number variation (CNV) in eEF2, PFDXR, PFPI4K, PFACRL, PFDHODH and PFCYTB respectively. HCl: Hydrochloric acid; *SYBR Green assay; PFEF2: *P. falciparum* translation elongation factor 2; PFDXR: *P. falciparum* 1-deoxy-D-xylulose-5-phosphate reductoisomerase; PFPI4K: *P. falciparum* phosphatidylinositol 4-kinase; PFCARL: *P. falciparum* cyclic amine resistance locus; PFDHODH: *P. falciparum* dihydroorotate dehydrogenase; PFCYTB: *P. falciparum* cytochrome b.

Table S1D. MMV688533 activity against *P. falciparum* liver and gamete stages.

Compound	Liver stage mean IC_{50}	Male gamete inhibition at 1 μM (mean ± SEM)	Male gamete inhibition at 1 μM (mean ± SEM)
MMV688533	4.0 μM[a]	-9.9 ± 2.2%[b]	2.0 ± 1.2%[b]

[a]Liver stage assays were conducted by the group of Dr. Koen Dechering at TropIQ Health Sciences, Nijmegen, The Netherlands. In this assay, the positive control atovaquone yields a mean ± SD IC_{50} value of 7 ± 4 nM (*66*). [b]Inhibition of male and female gametes was measured using the dual gamete-formation assay, as described (*67*). Assays were performed on three independent occasions with technical duplicates. The positive control thiostrepton, incubated at 2 μM for 48 h, yielded 100% and 63% inhibition of male and female gamete formation, respectively.

Table S1E. MMV688533 in vitro cytotoxicity IC_{50} (μM) on human cell lines and rat hepatocytes.

Salt	HL60	HepG2	Rat hepatocytes
HCl	13.1	> 15.6	15.0 (18.0 w/o BSA)

MMV688533 showed a selectivity of >1,000 against the three designated cell lines tested. There was also no swelling or depolarization on rat liver-isolated mitochondria at 62.5 μM. HCl: Hydrochloric acid; HL60: Human leukemia cell line; HepG2: Human liver carcinoma cells; w/o: without; BSA: Bovine Serum Albumin.

Table S1F. Summary of efficacy parameters from the *P. falciparum*-infected human red blood cell SCID mouse model study performed in recrudescence mode.

Assay	Parameter	Mean	95% Interval of confidence	Units
Non-standard 1-day	ED_{90}	2.0	1.9 - 2.1	mg/kg
Non-standard 1-day	AUC_{ED90}	3,097	2,335 - 4,484	ng.h/ml
Non-standard 1-day	AUC_{PCC}	8,046	3,802 - 12,511	ng.h/ml
Non-standard 1-day	C_{maxPCC}	382	231 - 576	ng/ml
Non-standard 1-day	AUC_{CURE}	> 193,123	-	ng.h/ml
Non-standard 1-day	$C_{maxCURE}$	> 5,506	-	ng/ml

Effective dose 90% (ED_{90}) and area under the curve 90% (AUC_{ED90}) are defined as the dose in mg/kg and the estimated average daily exposure, respectively, that reduce parasitemia by 90% on day 7 post-infection as compared to vehicle-treated mice. In this assay, this level of reduction implies no net parasite growth in blood. AUC_{PCC} and C_{maxPCC} is defined as the minimum average daily exposure (PCC, parasite clearance concentration) and maximal blood concentration (C_{max}) necessary to achieve maximum parasite clearance from peripheral blood. AUC_{CURE} and $C_{maxCURE}$ are defined as the minimum drug exposure and C_{max} in blood associated with cure of *P. falciparum*-infected SCID mice infused with human red blood cells.

Table S1G. Minimal parasiticidal concentration of MMV688533 in the *P. falciparum* infected NSG mouse model.

EC_{50} origin	EC_{50} (ng/mL)	MPC (EC_{90}) (ng/mL)
Final run #79865 (population estimate)	1.63	14.7
Bootstrap analysis: median [25,75% quantile] from n= 504 successful runs	2.25 [1.59;3.44]	20.3 [14.3;30.9][a]

The minimal parasiticidal concentration (MPC), was determined from the IC_{90} value of the killing curve plotted as a function of the circulating drug concentration and calculated from IC_{50} and the Hill coefficient. The MPC determined from either the IC50 estimate of the final PK/PD run or from the median IC_{50} of its related bootstrap analysis ranged between 14.7 and 20.2 ng/ml. a [25,75% quantile] for MPC deduced from [25,75% quantile] for IC_{50}.

Table S1H. MMV688533 in vitro metabolic clearances in microsomes and hepatocytes from different species.

Species	Liver microsomes CL_{int} (µL/min/mg)	Hepatocytes CL_{int} (µL/h/10^6cells)
Mouse	13	0-9
Rat	6.5	6-9
Dog	0	6
Macaque	0	15
Human	0	2

In vitro metabolic stability studies were performed using liver microsomes and cryopreserved hepatocytes of mouse, rat, dog, macaque or human origin. Results indicate low metabolic clearances in all species. CL_{int}: in vivo intrinsic clearance. Low liver microsome CL_{int} values are < 10 µL/min/mg, moderate values are between 10 and 50 µL/min/mg, and high values are > 50 µL/min/mg. Low hepatocyte CL_{int} values are < 4 mL/h/10^6 cells; moderate values are between 4 and 20 mL/h/10^6 cells; and high values are > 20 mL/h/10^6 cells.

Table S1I. MMV688533 inhibition of cytochromes P450 (CYP).

CYP enzyme	Selective substrate	IC_{50} (µM)	Mode of inhibition	K_i (µM)
CYP1A2	Phenacetin	no inhibition		
CYP2B6	Bupropion	56.4	Mixed	12.6
CYP2C8	Amodiaquine	1.6	Mixed	0.8
CYP2C9	Diclofenac	3.3	Mixed	2.4
CYP2C19	S-Mephenytoin	13.7	Mixed	9.0
CYP2D6	Dextromethorphan	10.6	Competitive	4.0
CYP3A4/5	Midazolam	8.2	Mixed	15.3
CYP3A4/5	Testosterone	27.3	Mixed	11.1

Data shown above were generated with purified CYP enzymes. When tested in vitro with human liver microsomes, MMV688533 did not inhibit CYP1A2, CYP2C9, CYP2C19, CYP2D6, and CYP3A at concentrations up to 10 µM.

Table S1J. MMV688533 pharmacokinetic parameters in male Swiss mice and male Sprague Dawley rats after intravenous and oral route administration.

Route	Dose (mg/kg)	Matrix	C_{max} (µg/mL)	AUC_{0-24} (µg.h/mL)	CL (L/h/kg)	V_{ss} (L/kg)	$T_{1/2}$ (h)	T_{max} (h)	F (%)	B/P
Male Swiss mice										
Intravenous	3	Plasma	6.14	10.3	0.29	1.36	3.2	-	-	-
Per os	3	Blood	0.86	11.7	-	-	4	8	-	-
Per os	10	Plasma	2.24	33	-	-	-	4	96	-
Per os	10	Blood	2.21	30	-	-	16	8	-	1.2
Per os	30	Blood	8.13	152	ND	ND	26	4	ND	ND
Male Sprague Dawley rats										
Intravenous	3	Blood	5.65	9.5	0.30	2.09	7.5	-	-	
Per os	10	Blood	1.14	22.8	-	-	9.6	4	71	

MMV688533 was administered by oral gavage (po, with compound suspended in methylcellulose/Tween 80 0.6%/0.5% in water) and by IV route as a solution using PEG200/ solutol/ G5% (20/5/75; w/w/v) to male Swiss mice (PKS10191-VA) and male Sprague Dawley rats respectively. Compound concentrations were determined by LC-MS/MS, with a Limit of Quantification (LOQ) of 2 ng/mL for plasma and 5 ng/mL for blood. (-) below the LOQ. In both species, the clearance (CL) is equivalent to the relatively low value of 0.005 µL/min/mg. In rodents, a T1/2 value (po) > 8h is considered as a long half-life when translated into humans. F (%), percent bioavailability. B/P, blood to plasma ratio. ND, not done.

Table S1K. MMV688533 pharmacokinetic parameters in male Sprague Dawley rats after oral administration.

Salt	Route	Dose (mg/kg)	Matrix	C_{max} (µg/mL)	T_{max} (h)	AUC_{0-168} (µg.h/mL)	AUC (µg.h/mL)	$T_{1/2}$ (h)	AUC ratio 300/30
Malonate	Per os	30	Blood	6.0	6	310	310	16	-
Malonate	Per os	300	Blood	30	48	2800	2800	38	9.1
Malonate	Per os	30	Brain	3.2	4	140	160	24	0.5*
Malonate	Per os	30	Liver	246	6	11000	11000	21	35*
Malonate	Per os	30	Heart	81	6	3200	3200	19	10*
Malonate	Per os	30	Kidney	182	4	7500	7500	16	24*
Malonate	Per os	30	Lung	439	24	17000	17000	16	55*

MMV688533 malonate salt was administered at 30 and 300 mg/kg by oral gavage (methylcellulose/Tween 80 0.6%/0.5% in water) to male Sprague Dawley rats. Concentrations were determined using LC-MS/MS, with a limit of quantification of 25 ng/ml for blood and 125 ng/g for tissues. At the 30 mg/kg dose level, the highest concentrations were reached at 6 h post-dosing and the exposures increased roughly proportionally with dose between 30 and 300 mg/kg for AUC exposure while C_{max} increased sub-proportionally with dose. The quantitative tissue distribution was also evaluated in brain, liver, lung, heart and kidney at the 30 mg/kg dose level after oral administration. Broad distribution of MMV688533 was observed with tissue/blood concentration ratios above 1 in all tissues except the brain. The T_{max} ranged mostly between 4 and 24 hours. The highest levels (tissue/blood concentration ratio = 55) were observed in lung > liver > kidney > heart > brain. Penetration into brain was significantly lower compared to penetration into other tissues. *Tissue:blood AUC ratio.

Table S1L. MMV688533 blood toxicokinetic parameters in male and female Sprague Dawley rats.

Sex	Dose (mg/kg/day)	Matrix	C_{max} (µg/mL)		T_{max} (h)		AUC_{0-24} (µg.h/mL)	
			Day 1	Day 4	Day 1	Day 4	Day 1	Day 4
Male	25	Blood	-	3.0	-	-	-	57.6
Male	50	Blood	-	8.9	-	-	-	188
Male	100	Blood	8.6	20.4	8	24	163	413
Female	25	Blood	-	5.2	-	-	-	99.4
Female	50	Blood	-	16.0	-	-	-	335
Female	100	Blood	10.1	17.9	24	24	195	355

MMV688533 maximal blood concentrations (C_{max}) were reached in females at 24 h post-dosing (last sampling time) and in males at 8 h post-dosing on Day 1 at 100 mg/kg. In females, MMV688533 Day 4 dose proportionality (C_{max} and AUC_{0-24}) over the 25-50 mg/kg/day dose range increased slightly supra-proportionally and were similar to the 50-100 mg/kg/day dose range. A 2-fold increase in dose (50 mg/kg/day vs 25 mg/kg/day) led to a 3.1-fold increase in C_{max} and a 3.4–fold increase in AUC_{0-24} and a further 2-fold increase in dose (100 mg/kg/day vs 50 mg/kg/day) led to a 1.1-fold increase in C_{max} and a 1.1–fold increase in AUC_{0-24}. In males, a slightly sub-proportional increase was observed. MMV688533 exposures increased in proportion over the 50-100 mg/kg/day dose range. A 2-fold increase in dose (50 mg/kg/day vs 25 mg/kg/day) led to a 3.0-fold increase in C_{max} and a 3.3–fold increase in AUC_{0-24}. A further 2-fold increase in dose (100 mg/kg/day vs 50 mg/kg/day) yielded a 2.3-fold increase in C_{max} and a 2.2–fold increase in AUC_{0-24}. At 100 mg/kg/day, MMV688533 mean accumulation ratios (D4/D1) in blood were 1.8 for both AUC_{0-24} and C_{max} in females and 2.5 AUC_{0-24} and 2.4 C_{max} in males. Based on MMV688533 C_{max} and AUC_{0-24} in blood, no gender effect was observed on Day 1. On Day 4, exposure in females was slightly higher with a female to male ratio ranging from 1.7 to 1.8 after dosing with 25 mg/kg/day or 50 mg/kg/day. No gender effect was observed at 100 mg/kg/day on Day 4, with a female to male ratio of 0.86 to 0.88. -, not determined. Two rats (one male and one female) were used per dose.

Table S1M. MMV688533 mean biliary and urinary excretion parameters in male Sprague Dawley rats.

	Excreted drug cumulated over 24 hours (% of administered dose)	
Period (h)	Bile	Urine
0-4	1.36 ± 0.28 (12)	-
0-8	1.48 ± 0.28 (19)	-
0-24	2.05 ± 0.38 (18)	2.22 ± 1.13 (51)

Biliary and urinary excretion was evaluated over 24 h after intravenous administration of 10 mg/kg MMV688533 as a solution of 40% Captisol in water to dual cannulated (bile duct and duodenum) male Sprague Dawley rats. An exploratory LC-MS/MS method with a limit of quantification of 1 ng/ml was used to quantify urine and bile samples. Data are shown as mean ± SD (CV%), from three rats. Low biliary and urine excretions were observed with around 2% of the administered dose being recovered after 24 h.

Table S1N. MMV688533 mean pharmacokinetic parameters in female Beagle dogs after intravenous injection.

Route	Dose (mg/kg)	Matrix	C_0 (µg/mL)	AUC_{0-72} (µg.h/mL)	AUC (µg.h/mL)	CL (L/h/kg)	V_{ss} (L/kg)	$T_{1/2}$ (h)
Intravenous	2	Blood	1.8	19.8	> 30%	0.07	4.74	50.7

MMV688533 was administered to 3 female Beagle dogs via intravenous route as a solution using PEG400/Ethanol/Solutol HS15/G5% (20/5/5/75) pH 3.0. Compound concentration was determined using LC-MS/MS. The limit of quantification was 5 ng/ml for blood. CL is equivalent to 0.011 µL/min/mg and is indicative of low clearance. In humans, compounds with a volume of distribution (V_{ss}) < 4 L are expected to be found exclusively in plasma. When V_{ss} is > 40 L, compounds are distributed in all tissues of the body and are almost absent in the plasma.

Table S1O. Mean blood pharmacokinetic parameters of MMV688533 and its metabolite RA14677213 following a single oral administration as capsule or oral solution to pentagastrin-induced male Beagle dogs.

Compound	Formulation	C_{max} (ng/mL)	T_{max} (min-max) (h)	AUC_{0-24} (µg.h/mL)	AUC_{0-168} (µg.h/mL)	AUC (µg.h/mL)	T_{last} (h)	$T_{1/2}$ (h)
MMV688533	Capsule	89.7	10.7 (2-24)	1.55	4.58	4.85	168	41
MMV688533	Solution	99.6	2.67 (2-4)	1.99	6.09	6.49	168	42.8
RA14677213	Capsule	19.9	3.33 (2-4)	0.36	1.13	1.24	168	51.5
RA14677213	Solution	22	5.33 (4-6)	0.405	1.38	1.54	168	51.6

The pharmacokinetics of MMV688533 and its metabolite RA14677213 were investigated in blood after a single 0.5 mg/kg dose that was orally administered to male Beagle pentagastrin-induced dogs. The solution formulation was at 0.25 mg/mL in PEG400/Ethanol/Solutol/G5% (20/5/7.5/67.5). The capsule formulation [MMV688533 /microcrystalline cellulose/croscarmellose sodium (5/91.67/3.33)] was followed by 50 ml water. 30 minutes before oral administration, the dogs were treated with pentagastrin (intra-muscular injection, 6 µg/kg, 0.25 mL/kg). The gastric pH was measured before dosing and was found to be < 3.0. MMV688533 and RA14677213 were quantified using LC-MS/MS with limits of quantification of 0.83 ng/ml and 1.0 ng/ml, respectively. Maximal MMV688533 blood concentrations were observed between 2-24 h for the capsule and between 2-4 h for the solution. MV688533 exposure observed after oral administration as capsule was around 25% lower compared to exposure observed after oral administration as solution. For RA14677213, the maximal blood concentrations were observed between 2-4 h for the capsule and between 4-6 h for the solution. Similar pharmacokinetic profiles were observed between MMV688533 and its metabolite. The elimination half-life for both capsule and solution formulations was ~40 h for MMV688533 and ~50 h for its metabolite. On average, RA14677213 represented around 22% of parent exposure for both formulations.

Table S1P. MMV688533 predicted human parameters.

Clearance (L/h)	$T_{1/2}$ (h)	V_{dss} (L)
Low: 3.6	103	5.0
Very low: 1.4	277	5.0

Mahmood rules and Fixed exponent method of allometric scaling of clearance from animal data predicted a low to a very low MMV688533 clearance (3.6 and 1.4 L/h (< 5%) of hepatic blood flow) in humans. This corresponded to a predicted half-life of 103 and 277 h respectively. The volume of distribution relying on allometry method with an exponent of 1 was predicted to be as high as 5.0L for a 70 kg individual.

Table S1Q. MMV688533 in silico prediction of genotoxicity/organ toxicity.

Toxicity	Derek	Leadscope	Internal toxicity results
Mutagenicity	No alert	No alert	No alert
Clastogenicity	No alert	No alert	No alert
Hepatotoxicty	No alert	Not relevant	To be monitored
Nephrotoxicity	No alert	Not applicable	To be monitored
Cardiac toxicity	No alert	Not applicable	To be monitored
Phototoxicity	No alert	moderate/low risks*	No alert

Knowledge-based approach using the software Derek and QSAR based (Leadscope) were used to predict in silico genotoxicity, hepatotoxicity, nephrotoxicity, cardiotoxicity and phototoxicity. (* moderate in vitro and low in vivo).

Table S1R. MMV688533 off-target activities.

Assay	IC_{50} (μM)
BZD (peripheral) (antagonist radioligand)	0.9
Ca^{2+} channel (L, dihydropyridine site) (antagonist radioligand)	1.1
Cl^- channel (GABA-gated) (antagonist radioligand)	4.3
Dopamine transporter (h) (antagonist radioligand)	9.4
Sigma (non-selective (h) (agonist radioligand)	4.8

Off target potential pharmacological activities of MMV688533 were assessed in a full CEREP profile on 19 enzymes (uptake assays), 88 receptors (binding assays), ion channels and amine transporters at 1 μM inhibition activity. The criterion for dose-response determination was "greater than 60% inhibition of activity or displacement of the labeled ligand". MMV688533 was found inactive at 1 μM on a panel of 315 kinases. Interactions of MMV688533 with receptors – although at very high concentrations – carry an alert for central nervous system and cardiovascular effects. These alerts have not been confirmed when assessed through in vivo experiments and GLP safety pharmacology testing prior to human clinical trials.

Table S1S. MMV688533 in vitro activity in µM on different cardiac ion channels.

Channel	Conc. (µM)
Potassium channel (hERG)	4.6
Sodium channel (Nav1.5)	14
Calcium channel (Cav1.1)	2.1

No cardiotoxicity alert was identified with MMV688533 from all the evaluated in vitro endpoints.

Table S1T. MMV688533 non-compartmental analysis of exposure in male Sprague Dawley rats.

Dose (mg/kg)	Mean male and Female $AUC_{0\text{-}24h}$ (ng.h/mL)	Cumulated AUC (ng.h/mL)
12.5	53,400	747,600
25	108,500	1,519,000

The steady-state $AUC_{0\text{-}24h}$ and cumulated AUC in 2-week toxicity studies were calculated using a non-compartmental analysis. Five animals per dose and sex were used to determine the concentration of MMV688533 in whole blood.

Table S1U. MMV688533 cumulated exposure over 14 days of treatment in Beagle dogs.

Dose (mg/kg)	Regimen	Total dose over 15 days (mg/kg)	AUC_{0-360h} individual values from non-parametric superposition (ng.h/mL)						Mean male + female (min-max) AUC_{0-360h}
			Male		mean	Female		mean	Male & Female
0.5	once daily	7.5	30,000	27,400	28,700	52,000	32,300	42,200	35,400 (27,400-52,000)
1.0	(QD)	15	76,600	87,700	82,200	67,400	86,000	76,700	79,400 (67,400-87,700)
2.0	once every 2 days (Q2D)	14	73,300	76,200	74,800	41,100	69,100	55,100	64,900 (41,100-76,200)

Cumulated AUC was calculated from 2-week toxicity studies using a population pharmacokinetic model.

Table S1V. Calculation of MMV688533 safety margin based on cumulative AUC over 14 days at the NOAEL dose in rats and dogs.

Species	Dose (mg/kg)	Mean AUC_{cum} (µg.h/mL)	Exposure (AUC_{0-inf}, µg.h/mL) of the human single dose (30 mg)	Therapeutic Index
Rat	12.5	747	5.7	>20
Dog	1.0	79	5.7	13.8

For rats the therapeutic index based on the cumulative AUC over 14 days at the NOAEL (No Observed Adverse Effect Level) dose of 12.5 mg/kg in rats, as compared with the AUC from an estimated single oral dose of 30 mg in humans, was estimated to be > 20. For dogs the therapeutic index calculated based on the cumulative AUC over 14 days at the NOAEL dose of 1 mg/kg in dogs, compared with the AUC from an estimated single oral dose of 30 mg in humans, was estimated to be 14. Whole blood exposure in humans was predicted based on compound efficacy in the Pf SCID mouse model and the calculated in vitro PRR of 3.0.

Table S2. Asexual blood stage IC_{50} data in nM of MMV688533-resistant parasite lines against common antimalarials.

	3D7-A10 wild type			ed. 3D7 ACG1^{G98V}			ed. 3D7 ACG1^{W286R}			sel. ed. 533-CL1$^{EHD-D218Y}$		
Compound	Mean IC_{50}	SEM	N	Mean IC_{50}	SEM	N	Mean IC_{50}	SEM	N	Mean IC_{50}	SEM	N
KAE609	0.7	0.1	3	0.7	0.0	3	0.6	0.02	3	0.7	0.04	3
Dihydroartemisinin	0.8	0.2	3	0.7	0.1	3	0.9	0.1	3	0.7	0.04	3
Lumefantrine	1.5	0.3	3	1.2	0.04	3	1.2	0.02	3	0.9	0.04	3
Chloroquine	5.5	1.0	3	6.2	0.1	3	8.3	1.1	3	9.2	1.5	3
Mefloquine	10.6	0.4	3	9.3	0.1	3	11.0	0.5	3	6.1	0.7	3
Ferroquine	6.5	1.3	3	8.1	0.4	3	11.5	1.9	3	12.1	2.6	3
Piperaquine	14.8	2.6	3	12.6	1.0	3	17.8	1.4	3	15.4	2.1	3
Quinine	24.5	3.7	3	22.2	1.3	3	25.2	2.6	3	15.4	0.8	3
md-amodiaquine	24.1	2.4	3	26.5	1.5	3	30.9	2.2	3	31.2	7.4	3
GNF179	45.7	9.1	3	42.4	7.1	3	55.0	11.2	3	35.1	7.4	3
Fosmidomycin	359	22	3	401	38	3	331	37	3	248	9.7	3

SEM: standard error of the mean; N: number of biological repeats (with technical duplicates). ed., gene edited. sel., selected under drug pressure.

Table S3: Protein functional pathway relationships.

Gene product	Gene ID	Protein ID	GO_component	GO_process	GO_function1	GO_function2
Conserved *Plasmodium* protein (PfACG1)	PF3D7_0910300	Q8I349_PLAF7	-	-	-	-
EH domain-containing protein (PfEHD)	PF3D7_0304200	Q9NLB8_PLAF7	vesicle	transport	heterocyclic compound	-
Conserved *Plasmodium* protein	PF3D7_0510100	Q8I403_PLAF7	-	-	heterocyclic compound	RNA binding
RNA pseudouridylate synthase, putative	PF3D7_0511500	Q8I3Z1_PLAF7	-	-	heterocyclic compound	RNA binding
ATP synthase (C/AC39) subunit, putative	PF3D7_1464700	Q8IKJ0_PLAF7	-	transport	heterocyclic compound	-

GO: Gene Ontology